Understanding the role of *paraxis* in *Nematostella vectensis* segmentation

A Thesis

submitted to

Indian Institute of Science Education and Research Pune in partial fulfillment of the requirements for the BS-MS Dual Degree Programme

by

Ritvee Rajendra Talele

Indian Institute of Science Education and Research Pune

Dr. Homi Bhabha Road,

Pashan, Pune 411008, INDIA.

Date: March 2024

Under the guidance of

Supervisor: **Dr. Matthew C. Gibson**,

Stowers Institute for Medical Research

From May 2023 to March 2024

INDIAN INSTITUTE OF SCIENCE EDUCATION AND RESEARCH PUNE

CERTIFICATE

This is to certify that this dissertation entitled “Understanding the role of *paraxis* in *Nematostella vectensis* segmentation” submitted towards the partial fulfillment of the BS-MS dual degree programme at the Indian Institute of Science Education and Research, Pune represents study/work carried out by Ritvee Rajendra Talele at the Stowers Institute for Medical Research under the supervision of Dr. Matthew Gibson during the academic year 2023-2024.

Dr. Matthew Gibson

Committee:

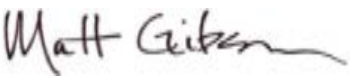

Dr. Matthew Gibson

Dr. Richa Rikhy

This thesis is dedicated to my parents who sparked my interest in Biology

DECLARATION

I hereby declare that the matter embodied in the report entitled “Understanding the role of *paraxis* in *Nematostella vectensis* segmentation” are the results of the work carried out by me at the Stowers Institute for Medical Research, under the supervision of Dr. Matthew Gibson, and the same has not been submitted elsewhere for any other degree. Wherever others contribute, every effort is made to indicate this clearly, with due reference to the literature and acknowledgement of collaborative research and discussions.

Ritvee Rajendra Talele
20191036

TABLE OF CONTENTS

LIST OF TABLES

LIST OF FIGURES

ABSTRACT

Segmentation is a feature of all bilaterian chordates. It is initiated in the early embryo through a process called somitogenesis. The paraxial mesoderm, composed of mesenchymal cells, gives rise to repeated epithelial structures called somites through a mesenchymal-to-epithelial transition. In contrast, the endoderm of the cnidarian sea anemone, *Nematostella vectensis,* is divided into eight bi-radially positioned segments. Cnidarians are the sister group to bilaterians and like all its members, *N. vectensis* is diploblastic, containing only two germ layers, and lacking a well-defined mesoderm. Yet, surprisingly, the *Nematostella* endoderm expresses several genes whose bilaterian orthologs are typically involved in mesoderm patterning and vertebrate somitogenesis. Moreover, several morphological parallels exist between *Nematostella* segments and vertebrate somites. Taken together, this hints at the possibility of a common origin between the two, suggesting that the molecular mechanisms involved in segmentation were likely present in the last common ancestor of bilateria and cnidaria more than 600 million years ago.

This thesis aims to understand the role of *paraxis* in *N. vectensis* segmentation, which is orthologous to a vertebrate somitogenesis factor of the same name. In vertebrates, *Paraxis* is a bHLH transcriptional activator that regulates the mesenchymal-to-epithelial transition of somites and is crucial for somite epithelialization. *Paraxis* knockout mice display defects in formation of the axial skeleton and somite derivatives during early development and lethality follows shortly after birth.

Using an shRNA-mediated gene knockdown approach, the results presented here indicate that in *Nematostella, paraxis* regulates the organization of cells within the endomesodermal segments. *Paraxis* knockdown leads to a partial or complete loss of segment boundaries, suggesting that it might be involved in the segmentation program, however, its role in *N. vectensis* remains unknown.

ACKNOWLEDGEMENT

First and foremost, I would like to thank my supervisor, Dr. Matt Gibson, for believing in me throughout my Masters' project and for his constant support and guidance. Moreover, I would like to thank Emma, my mentor, who patiently taught me all the techniques and helped me troubleshoot my experiments. I thank all members of the Gibson lab, Whitney, Lacey, Steffi, Dilan, Jenny, Christof, Rouhan, Anna, Anne, and Abby for being so welcoming and helpful.

I thank Dr. Richa Rikhy for encouraging me to take this opportunity and initiating my interest in developmental biology through courses in Genetics and Developmental Biology and the semester projects under her guidance.

I am grateful to my flatmates, Amisha and Shruti, for being the bits of familiarity in a new country and all the times we cooked together. Despite being in different timezones, talking to my friends from IISER always made my days a bit better; I would like to particularly thank Vidisha, Abhisek, Sakshi, Akash and Manav among others for staying in touch and checking in.

Lastly, I would like to thank my parents, and my sister, without whom I would not have been here. I am grateful for their support and their trust. I love you.

CONTRIBUTIONS

Contributor name	Contributor role
Dr, Matt Gibson	Conceptualization Ideas
Dr. Matt Gibson, Dr. Emma Rangel-Huerta, Ritvee Talele	Methodology
-	Software
Ritvee Talele	Validation
Ritvee Talele	Formal analysis
Ritvee Talele	Investigation
Stowers Institute for Medical Research	Resources
-	Data Curation
Ritvee Talele	Writing - original draft preparation
Dr. Matt Gibson, Dr. Emma Rangel-Huerta	Writing - review and editing
Ritvee Talele	Visualization
Dr. Matt Gibson	Supervision
Dr. Matt Gibson	Project administration
Dr. Matt Gibson	Funding acquisition

This contributor syntax is based on the Journal of Cell Science CRediT Taxonomy[1].

[1] https://journals.biologists.com/jcs/pages/author-contributions

CHAPTER 1: INTRODUCTION

> "It is difficult to find a [concept] in the whole of zoology that is so vaguely defined, but, at the same time, so universally employed as…metamerism."
>
> RB Clark, 1964 (Hannibal & Patel, 2013)

The dramatic ecological and evolutionary events prior to and during the Cambrian explosion nearly 530 million years ago led to the emergence of diverse body plans. During this period of early evolution, animals evolved organs and organ systems and an orderly repetition of body parts known as segmentation, which eventually led to the specialization of metameric structures and the diversification of metazoan lineages. (Zhang & Shu, 2021)

For over 2,000 years, animals have been described as segmented, consisting of repeated units along the body axis. The evolutionary success of the major bilaterian lineages (annelids, arthropods, and chordates) is attributed to their segmented trunk region, which enhances locomotion and feeding. Although segmentation through somitogenesis (see 1.1) is common in all chordates (segmentation in other bilaterians is out of the scope of this thesis), developmental differences raise questions about the origins of somitogenesis.

In 1884, Adam Sedgwick proposed a theory known as the 'enterocoel' theory, indicating that cnidarians, the phylogenetic sister group to bilaterians, could provide the answer to the evolutionary origins of somites. According to this theory, the gastric pouches in cnidarians represent a rudimentary form of somites (Onai et al., 2015). It imagines an evolutionary scenario in which a diploblast, radially symmetric ancestor consisting of at least four gastric pockets, developed a new axis along one pair of gastric pouches perpendicular to the oral-aboral axis. The elongation of the oral opening along the newly formed axis led to the separation of the gastric pouches to form coelomic sacs (Tautz, 2004). The two ends of the newly formed axis will eventually form the mouth and the

anus. However, considerable debate exists around this hypothesis due to the lack of genetic and molecular evidence.

1.1 Somitogenesis

The segmentation process in vertebrates is initiated in the early developing embryo by forming metameric epithelial structures called somites (Gibb et al., 2010; Piatkowska et al., 2021), which further develop into the axial skeleton, musculature, and an organized peripheral nervous system. Somites progressively bud off in pairs from the anterior end of the presomitic mesoderm (PSM) located on either side of the neural tube (Figure 1.1). The PSM tissue is continuously replenished by cells from a posteriorly located region called the tail bud (Gibb et al., 2010), which contains a population of embryonic stem cells. Thus, somites are formed as the body axis extends at the posterior end.

The PSM is composed of loosely organized mesenchymal cells; however, individual somites are formed after a mesenchymal-to-epithelial transition (MET) and contain elongated, columnar epithelial cells (Figure 1.1) arranged radially around a center filled with unorganized mesenchymal cells (Takahashi & Sato, 2008).

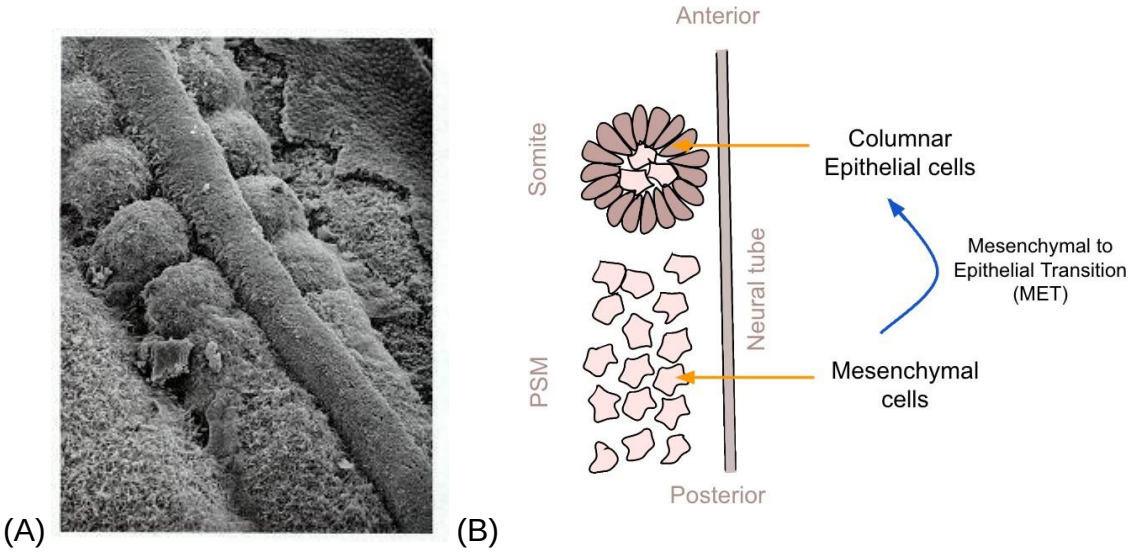

Figure 1.1: (A) Scanning Electron Micrograph showing central neural tube, individual somites, and the paraxial mesoderm (bottom right) that has not yet separated into somites. (Image from Gilbert SF. Developmental Biology. 6th edition. 2000). (B) Schematic showing the cell types that comprise the paraxial mesoderm and the individual somites.

The molecular mechanism of somitogenesis is well studied and is described by the clock and wavefront model (Carraco et al., 2022; Cooke & Zeeman, 1976), which produces somites in a temporally and spatially regulated manner (Figure 1.2). The clock comprises genes from the HES family of transcription factors and signaling pathways, including the Notch, Wnt and FGF signaling pathways. These clock genes oscillate in the PSM in a cell-autonomous fashion, generating a cell-responsive state. The specific oscillating gene varies between species and has been identified as *hairy1* in the chick embryo, *Hes7* in mice, and *her1* along with *her7* in zebrafish (Gibb et al., 2010); however, the fundamental feature of the embryonic clock remains the same. A negative feedback loop and the inhibitory action of HES protein on its promoter maintain the oscillation. The wavefront is defined by a posterior-to-anterior gradient of FGF and Wnt and an opposing anterior-posterior gradient of Retinoic Acid (RA) (Carraco et al., 2022). When the wavefront of determination meets the cell-responsive state produced by the clock gene oscillations, somitic boundaries are formed.

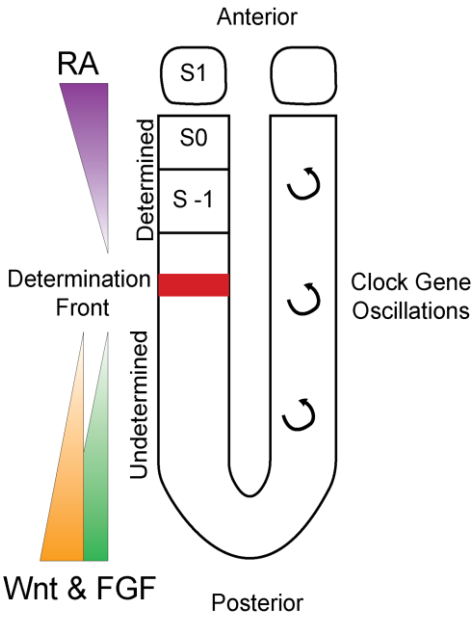

Figure 1.2: Schematic showing the clock and wavefront model that produces somite boundaries (represented in red). Modified from Gibb et al., 2010.

The cells within the somite are designated to their respective fates as the somite matures. Cells closest to the neural tube form the sclerotome that gives rise to the cartilage and vertebrae (Gilbert, 2000). The rest of the somite forms a double-layered epithelial structure called the dermomyotome; the lower layer forms the myotome, giving rise to the epaxial and hypaxial muscles. The central region of the dermomyotome's dorsal layer, the dermatome, gives rise to the dermis of the back (Gilbert, 2000).

Initially, the sclerotome and dermomyotome are part of the same somite; however, to form the vertebrae, the sclerotome shifts with respect to the dermomyotome. According to the resegmentation shift model (Ward et al., 2017), each vertebra is formed when half a sclerotome from one somite joins another half-sclerotome from the adjacent somite (Figure 1.3).

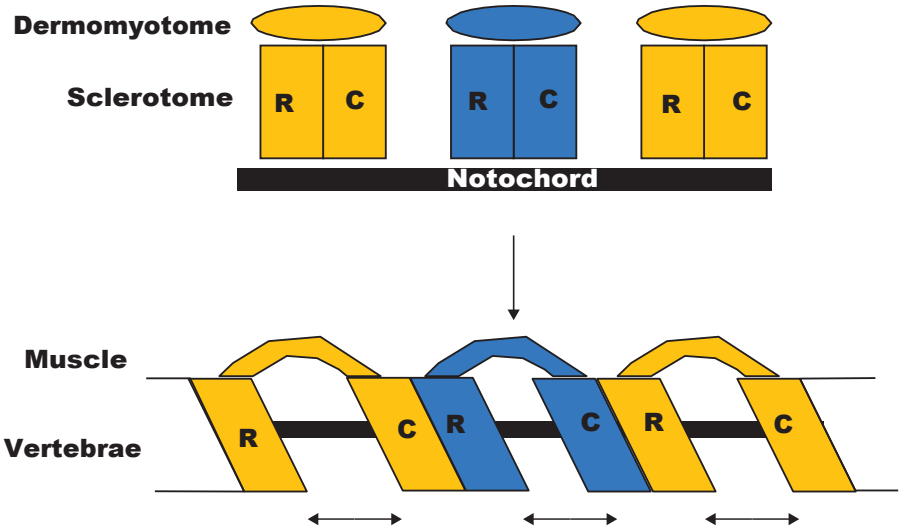

Figure 1.3: Schematic showing the resegmentation-shift model for formation of vertebrae as the caudal half of one somite joins the rostral half of the adjacent somite accompanied by a shift of variable extent along the axis (arrows). Modified from Ward et al., 2017.

1.2 Cnidarians as a model to understand the evolution of bilaterian traits

The astonishing diversity of bilaterian animals led researchers to ask questions about the evolution of bilaterian traits (like segmentation) and the morphological and molecular "starting points" of these traits. To answer this question, evolutionary biologists attempted to identify traits that were likely present in the common ancestor of all bilaterians by comparing them to non-bilaterian animals. Widely accepted as the sister group to bilaterians (Figure 1.3), cnidarians are an attractive target for studying the evolution of key bilaterian traits (Layden et al., 2016; Technau & Steele, 2011).

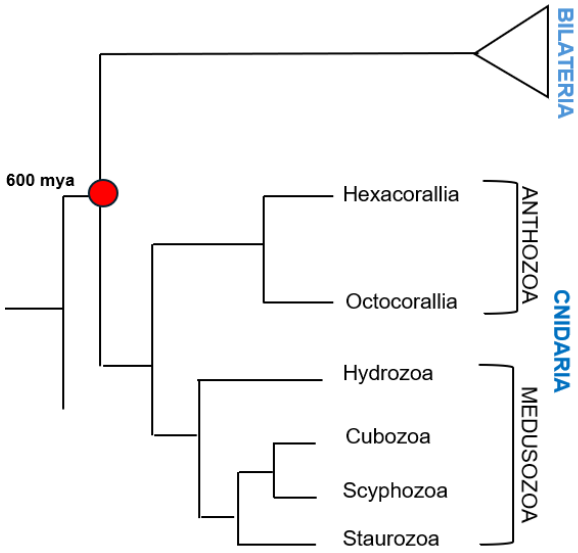

Figure 1.4: Phylogenetic tree showing Cnidaria as an outgroup to Bilateria and the two major classes within Cnidaria - Anthozoa and Medusozoa. Modified from Technau & Steele, 2011.

Cnidarians (corals, jellyfish, sea anemones, and hydroids) form a diverse phylum living primarily in marine environments. The phylum is divided into two major groups: the Anthozoa, which lives as a sessile polyp, and the Medusozoa (Figure 1.3), many of which (not all) undergo a free-swimming medusa stage in their life cycle (Technau & Steele, 2011). All cnidarians possess stinging cells called cnidocytes, which gives the

phylum its name. Cnidocytes are specialized cells used for predation, adhesion, and self-defense (Technau & Steele, 2011).

Traditionally, cnidarians have been considered radially symmetric. However, anthozoans have been known to possess an internal bilateral symmetry, giving rise to a secondary body axis called the directive axis, orthogonal to the long oral-aboral axis, and running along the slit-like pharynx (Finnerty et al., 2004; Saina et al., 2009). All cnidarians are diploblastic, i.e., they possess two germ layers (ectoderm and endomesoderm) and lack a well-separated mesoderm. Unlike bilaterians with a centralized nervous system, cnidarian animals have a simple diffused nervous system (Technau & Steele, 2011). These features distinguish the body plan of bilaterians and cnidarians, indicating the key evolutionary differences in the bilaterian lineage after the phyla split from its common ancestor more than 600 million years ago.

1.3 *Nematostella vectensis*: a cnidarian model system

Nematostella vectensis belongs to the anthozoan class of cnidarians and lives in an estuarine environment. It is, therefore, naturally exposed to fluctuations in temperature and salinity (Röttinger, 2021). Being the first cnidarian to have its genome sequenced, transcriptomic profiles are available for various developmental stages and tissues (Putnam et al., 2007), allowing studies on comparative genomic analysis. As a model organism, *Nematostella* has numerous advantages. It is a broadcast spawner, making it possible to collect a large number of gametes at a time. The rapid embryonic and larval development enables the visualization and manipulation of the embryos. Over the years, several protocols have been established, including laboratory maintenance and spawning (Genikhovich & Technau, 2009), microinjection and electroporation of short-hairpin and morpholino-based gene knockdown ((He et al., 2018; Karabulut et al., 2019; Layden et al., 2013) and CRISPR/Cas based gene editing (Ikmi et al., 2014).

Nematostella follows a typical anthozoan life cycle (Figure 1.4). Although there is no sexual dimorphism, it is dioecious and can reproduce sexually (Fritzenwanker et al., 2007; Layden et al., 2016). Fertilization occurs in an external environment after spawning, and the resulting zygote undergoes cleavage with a highly variable pattern (Fritzenwanker et al., 2007). At 24 hours post-fertilization (hpf), the gastrula develops into the free-swimming planula stage, lasting until 96 hpf. Over the course of a week, the planula gradually elongates and undergoes a metamorphosis characterized by an arrest in swimming and the formation of the first four tentacle buds of the primary polyp (Layden et al., 2016; Röttinger, 2021; Technau & Steele, 2011). The primary polyps grow and mature in a nutrient-dependent manner, adding more tentacles until they reach sexual maturity (Layden et al., 2016).

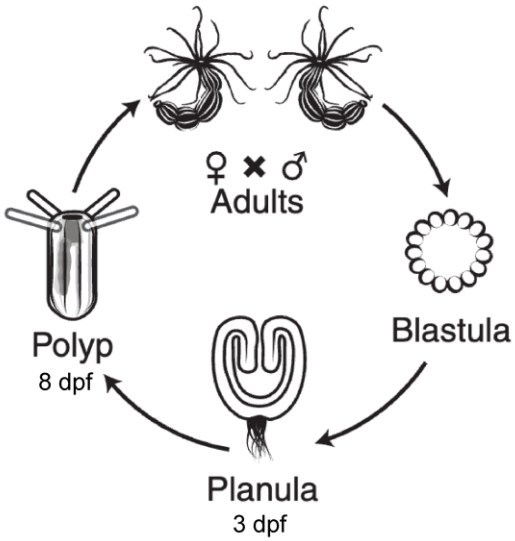

Figure 1.5: Schematic for the life cycle of *N. vectensis*. The embryos form a free-swimming planula stage after approximately 48 hours post-fertilization. Taken from He et al., 2018.

Morphologically, *Nematostella* planula larvae have two germ layers (Steinmetz et al., 2017). These are the ectoderm, which develops into the outer epidermis, and the endoderm, which develops into the inner gastrodermis. The mesoglea, a largely acellular matrix containing few ameboid cells, separates the two germ layers. They possess a sac-like gut and consist of a single oral opening corresponding to the site of gastrulation (Layden et al., 2016). In the juvenile and adult stage, the pharynx and eight radially arranged mesenteries are patterned along the long oral-aboral axis. Up to 16

tentacles surround the adult mouth and are used for capturing prey and feeding (Layden et al., 2016).

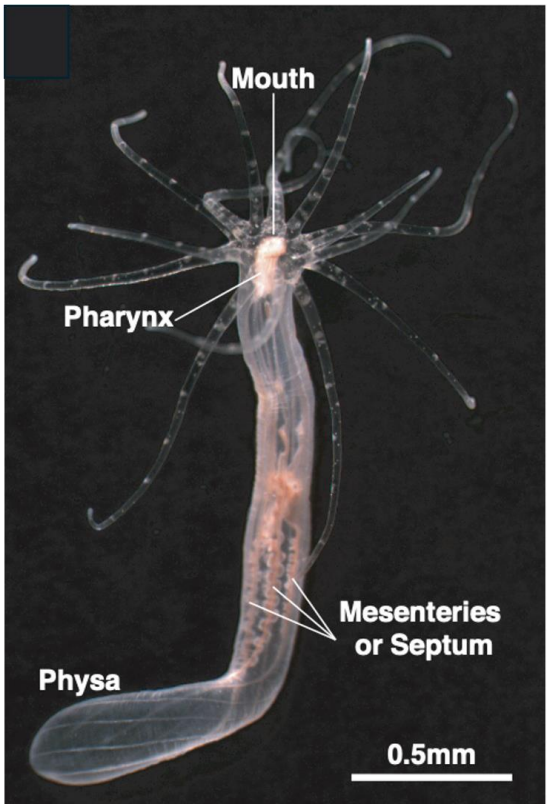

Figure 1.6: Adult *N. vectensis* morphology. Image from Layden, M. J., Rentzsch, F., & Röttinger, E. (2016).

Unfertilized oocytes do not possess a polarity; however, post-fertilization, the reorganization of egg cytoplasm leads to the selective degradation of β-catenin at the future aboral pole and its stabilization and nuclear localization in the endoderm forming pole, which marks the site of gastrulation (Wikramanayake et al., 2003). The resulting blastopore gives rise to the future head of the polyp. Although the role of Wnt/β-catenin signaling in the initial establishment of the oral-aboral axis remains unclear, a staggered expression of individual Wnt genes in the oral half of the embryo at mid-blastula stage suggests the involvement of the Wnt/β-catenin signaling pathway in the subsequent patterning of the long axis (Fritzenwanker et al., 2007).

The directive axis, which runs orthogonal to the oral-aboral axis, is patterned by BMP signaling. At the onset of gastrulation, negative feedback from BMP signaling causes a symmetry break in the radial expression of the BMP molecule, *NvDpp* and its antagonist *NvChd*, resulting in their localization on one side of the blastopore (Figure 1.7) (Genikhovich et al., 2015; Saina et al., 2009). The peak of BMP signaling occurs at a maximum distance from the source of *NvDpp*, forming a signaling gradient along the directive axis (Genikhovich et al., 2015).

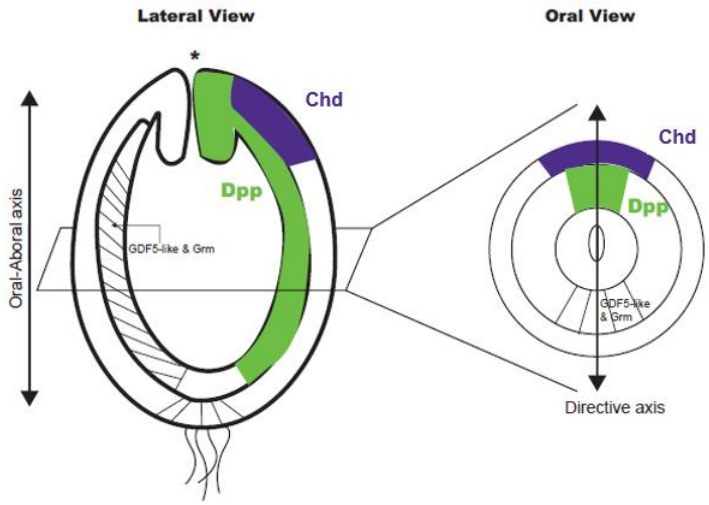

Figure 1.7: The directive axis is patterned by asymmetric expression of *NvChd* and *NvDpp*. The lateral view shoes expression of *NvChd* is on one side of the blastopore (marked by asterisk) and *NvDpp* in the blastopore lip on the same side and in the endoderm. Modified from Genikhovich et al., 2015.

During the early planula stage, the developing endoderm undergoes morphological segmentation giving rise to eight bi-radially positioned segments (numbered S1 to S8) along the directive axis (He et al., 2018; Technau & Genikhovich, 2018). These segment boundaries precisely correspond to the position of the eight mesenteries. Furthermore, the even-numbered segments develop into the first four tentacles of the primary polyp. He et al., 2018 have shown that under the control of BMP signaling, *Anthox1a*, *Anthox6a*, and *Anthox8*, along with *Gbx*, exhibit sharp expression territories (Figure 1.6(A)) corresponding to the position of the segment boundaries. Knockdown of

individual Hox genes leads to specific fusion of segments and defects in tentacle patterning (He et al., 2018), suggesting that the formation of segment boundaries is controlled by a Hox-Gbx code (Figure 1.6(B)).

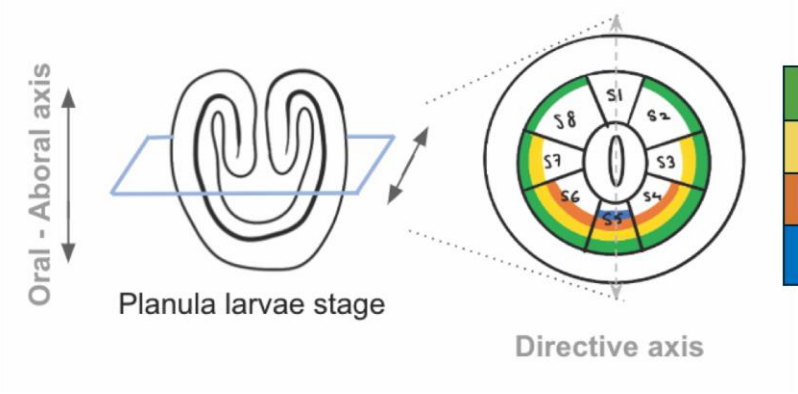

(A)

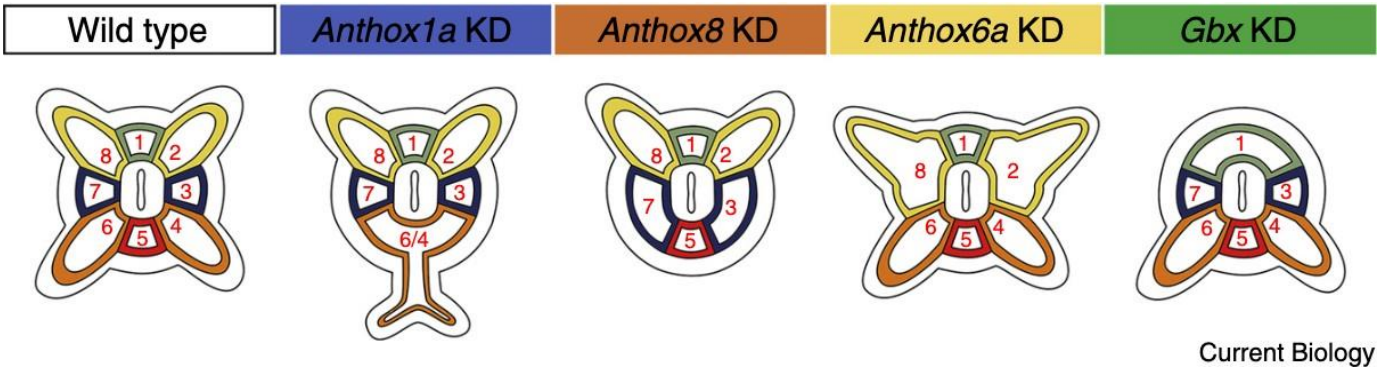

(B)

Figure 1.8: (A) Overlapping expression of Hox-Gbx genes regulates the formation of segment boundaries in *Nematostella.* (B) Fusion of segments and tentacle patterning defects observed in Hox-Gbx knockdown in juvenile polyps. Taken from Technau & Genikhovich et al., 2015.

Counteracting signals from the Hox-Gbx genes and the BMP gradient are responsible for the segmentally polarized gene expression of two conserved homeobox-containing genes *Lbx* and *Uncx* (He et al., 2023). Interestingly, they have both been described as segment polarity genes in different bilaterians. *Uncx* is found in the posterior boundary of vertebrate somites whereas *lbx/ladybird* is expressed in the posterior boundary of annelids (Steinmetz et.al., 2023). The polarization of segments is evident by the position

of four pairs of longitudinal retractor muscles (Figure 1.7), three on the Uncx side and one on the Lbx side (He et al., 2023).

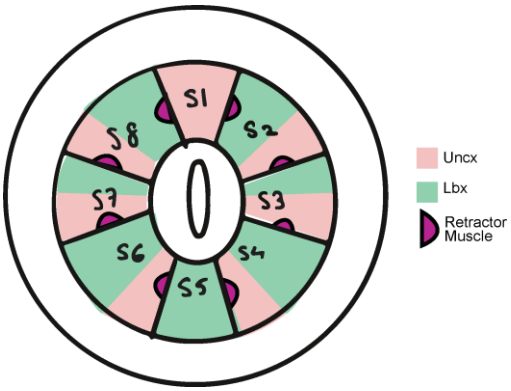

Figure 1.9: Schematic showing the polarized expression of *Uncx* and *Lbx* and retractor muscles patterned in a segmentally polarized manner. Three pairs of retractor muscles are patterned on the Lbx side and one pair along the Uncx side. Modified from He et al., 2023.

The regulation of Hox genes by the BMP signaling gradient in early axis patterning is unusual in Bilaterians, where BMP signaling is known to pattern the dorsoventral axis, whereas a staggered Hox gene expression is observed along the anterior-posterior axis and plays a role in establishing segment identity along this axis. It is, therefore, difficult to make homology assumptions between the body axes in bilaterians and those in cnidarians.

Interestingly, the *Nematostella* endoderm is found to be enriched with orthologs of bilaterian genes (Steinmetz et al., 2017) important for patterning the mesoderm (*foxC, six4/5*), skeletal muscles (*eyesabsent/eya, six1/2, six4/5, lbx/ladybird*) and vertebrate somites (*paraxis/scleraxis, tbx15/18/22, twist, mox*). Together, these genes argue for a complex molecular nature of *Nematostella* endomesoderm segments (He et al., 2023).

1.4 Hypothesis: *Nematostella* segments are homologous to vertebrate somites

The enterocoel theory, which imagines that the cnidarian gastric pouches represent a rudimentary form of somites, along with the striking similarities in the design principles, both molecular and morphological, between *Nematostella* segments and vertebrate somites, make it tempting to think that there exists a homology between them. Integrative approaches for assessing homology are often better than arguing for homology solely based on either morphology/phylogeny or developmental genetics (Nejad Kourki, 2022).

It is easy to see the morphological similarities between somites and *Nematostella* segments. They are both clusters of epithelial cells patterned along a body axis: the anterior-posterior axis in the case of somites and the directive axis in the case of *Nematostella* segments. Each possesses a segmental polarity integral to patterning adult body structures and tissues (He et al., 2023). In terms of genetic/molecular similarities, recent studies have shown that *Nematostella* segments express genes whose orthologs are important in the formation of vertebrate somites (Steinmetz et al., 2017). This thesis focuses on understanding the function of one of these gene orthologs, *paraxis*, a bHLH transcription factor, involved in the mesenchymal-to-epithelial transition of vertebrate somites and expressed in the endomesoderm of *Nematostella*.

1.5 Role of *paraxis* in mice

Paraxis is a basic helix-loop-helix (bHLH) transcription factor belonging to the twist subfamily of transcription factors (Wilson-Rawls et al., 2004). The bHLH superfamily regulates critical developmental processes, including neurogenesis, myogenesis, chondrogenesis, etc. They possess a highly conserved functional domain consisting of two amphipathic alpha helices separated by a loop region (Wilson-Rawls et al., 2004).

Paraxis is expressed in the anterior pre-somitic mesoderm and throughout the somites in the chick, mouse, and zebrafish embryos (Rowton et al., 2013; Šošić et al., 1997; Wilson-Rawls et al., 2004). As the somites mature and compartmentalize, *paraxis* gets restricted to the dermomyotome region.

The early expression of *paraxis* is regulated by Wnt6 signals from the surface ectoderm that act through the canonical Wnt/β-catenin pathway (Piatkowska et al., 2021; Rowton et al., 2013; Šošić et al., 1997). *Paraxis* expression is lost on removal of the surface ectoderm, and somites fail to epithelialize. Separating the PSM from the neural tube does not affect the initial expression of *paraxis*; however, its expression reduces after 24 hours, suggesting that signals from the neural tube, along with those from the surface ectoderm, maintain late expression of *paraxis* in the developing somites (Šošić et al., 1997).

In the absence of *paraxis*, mice show a caudal truncation of the axial skeleton and a fusion of the ribs (Burgess et al., 1996). Lethality follows shortly after birth and is mainly due to defects in the patterning of somite derivatives ((Burgess et al., 1996). *Paraxis* is involved in the mesenchymal-to-epithelial transition during somite formation (Rowton et al., 2013). In its absence, somites fail to epithelialize, leading to a loss in the anterior-posterior polarity of the somite. Adherens junction markers such as N-cadherin and Rho GTPase (RHOA), which are typically localized in the apical surface of the dorsal epithelium of wild-type mice, are mislocalized in somites of *paraxis* -/- mice (Rowton et

al., 2013), indicating its role in maintaining apical/basal polarity within the epithelial somites.

Paraxis is a transcriptional activator and can bind to E-box elements (Wilson-Rawls et al., 2004) by forming heterodimers with E-proteins to activate target genes. Rowton et al., 2013 observed the downregulation of genes associated with stabilizing the extracellular matrix (ECM), cell adhesion, cytoskeleton organization, and cell signaling in *paraxis* -/- mutant somites. Additionally, actin filaments that regulate the cytoskeleton and provide structural support for cell adhesion were mislocalized in *paraxis* -/- somites. Defects in the formation of hypaxial and epaxial muscles have also been reported in the absence of *paraxis* (Wilson-Rawls et al., 1999).

Evidence from *Xenopus laevis* further highlights the developmental importance of *paraxis* in regulating cell behavior during somite formation. In anurans like *Xenopus laevis*, somites are formed through a rotation of blocks of cells of the PSM. Despite the lack of epithelialized somites in anurans, a loss of *paraxis* in *Xenopus* embryos leads to a dramatic disorganization of somite tissue and affects somite morphology (Sánchez & Sánchez, 2015).

1.6 Paraxis in *Nematostella vectensis*

Cnidarians are reported to contain several members of bHLH transcription factors belonging to orthologous families such as ASCa, Twist, and SCL. (Gyoja, 2017) . The presence of bHLH genes in bilaterian and cnidarian genomes indicates that these genes were present in the last common ancestor of bilaterians and cnidarians, the urbilaterian ancestor (Simionato et al., 2007).

The cnidarian *paraxis* homolog is expressed in *Nematostella* endoderm (Steinmetz et al., 2017). According to spatial gene expression patterns, *paraxis* is expressed within the eight segments of the *Nematostella* planula endoderm. Gene expression patterns can be predicted by the *in silico* gene expression atlas (EndoAtlas) constructed by integrating computational approaches with single-cell transcriptomic data such that cells in physical proximity are expected to have similar transcriptomic profiles (He et al., 2023).

However, the function of *paraxis* in driving segment formation or maintenance remains unknown. This thesis aims to understand the role of *paraxis* in segmentation by a simple shRNA-based gene knockdown approach.

CHAPTER 2: MATERIALS & METHODS

2.1 MATERIALS:

2.1.1 Antibodies

Name	Host	Type	Source
Phalloidin 488	-	-	ThermoFisher #A12379
NvDlg	Rabbit	polyclonal	Genscript, custom-made
Hoechst 34580	-	-	Sigma #63493
Rabbit 488, secondary	Goat	polyclonal	ThermoFisher #A-11008
Anti-Digoxigenin-POD (DIG), Fab fragments	Sheep	polyclonal	Sigma, #11207733910
Anti-Digoxigenin-AP (DIG), Fab fragments	Sheep	polyclonal	Sigma, #11093274910

2.1.2 Enzymes and Reagents

Name	Source
Direct-zol™ RNA Miniprep Plus Kit	Zymo Research #R2072
Zymoclean™ Gel DNA Recovery Kit	Zymo Research #D4002
DNA Clean & Concentrator-5	Zymo Research #D4013

AmpliScribe™ T7-Flash Transcription Kit	Lucigen ASF3507
DIG RNA Labeling Mix	Roche #11277073910
T7 RNA Polymerase	Promega #171136
TSA Plus Cyanine 3 (Cy3) detection kit	Akoya Biosciences NEL 744001KT
BCIP/NBT Color developing reagent	Promega S3771
Blocking Reagent	Roche #46925300
Dextran, Texas Red; 3000 MW	Life Tech #D3328
FITC	ThermoFisher #46425

2.1.3 Genes used

Name	**Gene ID (NV2)**	**Gene ID (UVienna)**	**References**
Paraxis (tcf15)	NV2.10865	NVE19720	He. et al., 2023

2.1.4 Oligonucleotides used

Name	**Sequence (5’-3’)**
sh-Paraxis1 Forward primer	TAATACGACTCACTATAGGACTCGGATAGCTCTC TAATTCAAGAGATTAGAGAGCTATCCGAGTCTT

sh-Paraxis1 Reverse primer	AAGACTCGGATAGCTCTCTAATCTCTTGAATTAGA GAGCTATCCGAGTCCTATAGTGAGTCGTATTA
sh-Paraxis2 Forward primer	TAATACGACTCACTATAGGAACGCCAGTCGATTG AAATTCAAGAGATTTCAATCGACTGGCGTTCTT
sh-Paraxis2 Reverse primer	AAGAACGCCAGTCGATTGAAATCTCTTGAATTTCA ATCGACTGGCGTTCCTATAGTGAGTCGTATTA
ParaxisProbe(a) Forward primer	ATGGAAGGAACGAGAAGAAAGCGA
ParaxisProbe(a) Reverse primer	TCTCTCCGAGGAGCACCGTATT
ParaxisProbe(a) T7 reverse primer	ATAATACGACTCACTATAGGTCTCTCCGAGGAGC ACCGTATT
ParaxisProbe(b) Forward primer	CGAGAAGAAAGCGAGAACGC
ParaxisProbe(b) Reverse primer	TCCGATTCCCCATACTCCCA
ParaxisProbe(b) T7 reverse primer	ATAATACGACTCACTATAGGTCCGATTCCCCATAC TCCCA

2.1.5 Software and Algorithms

Name	**Source**	
Nematostella Genome	SIMR base	https://simrbase.stowers.org/starlets eaanemone
InvivoGen siRNA Wizard™	Web interface	https://www.invivogen.com/sirnawiza rd/index.php
EndoAtlas	He et al., 2023	http://simrbase.stowers.org:8888/

2.2 METHODS

2.2.1 Animal husbandry and spawning

Nematostella animals were housed at the Stowers Institute Aquatics facility in 12 parts per thousand (ppt) artificial seawater (ASW) and fed regularly with freshly hatched artemia brine shrimp. Spawning was carried out by subjecting sexually mature male and female colonies to a light shock followed by a cold shock to induce gamete production (Stefanik et al., 2013). Egg sacs were then de-jellied using a cysteine solution as described in (Genikhovich & Technau, 2009).

2.2.2 Synthesis of shRNA

Short hairpin RNA (shRNA) mimics the precursor microRNA (pre-miRNA) during endogenous microRNA (miRNA) processing, which regulates the expression of messenger RNA (mRNA) in most plants and animals. Enzymes, including Dicer, process the miRNA, and the functional strand is eventually loaded onto the RNA-induced silencing complex (RISC) (He et al., 2018; Moran et al., 2014). The active RISC complex binds to the target mRNA through partial or complete complementarity, repressing the expression of target mRNA and effectively leading to the silencing of gene expression (Figure 2.1).

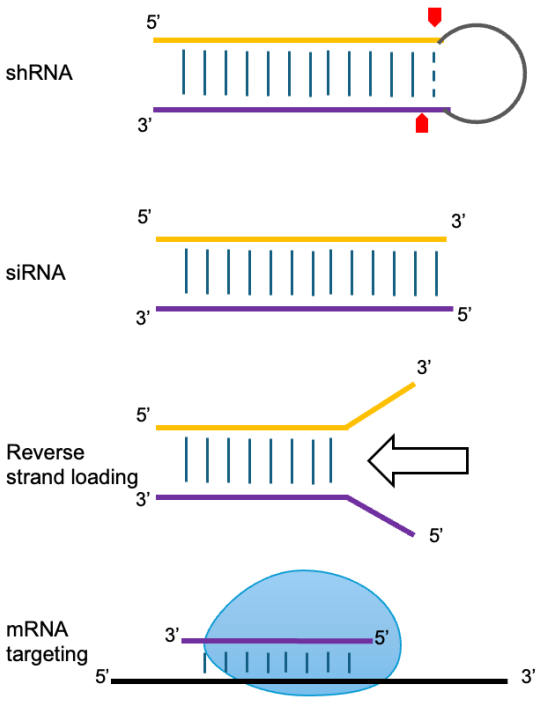

Figure 2.1: Mechanism of targeting of mRNA by shRNA through an activated RISC complex (in blue). Modified from He et al., 2018.

For shRNA design, the mRNA nucleotide sequence for the gene of interest, obtained from SIMRbase, was submitted to Invivogen siRNA Wizard^{TM} web (see materials) interface with motif size set to 19 nucleotides. Candidate sequences with 40-55% GC content were selected and BLASTed against the *Nematostella* genome to check for gene specificity. A 9 nucleotide loop sequence (5'TTCAAGAGA3') was introduced between the forward and reverse stems to construct the full-length shRNA sequence (Hill et al., 2022; Karabulut et al., 2019). The forward and reverse primers were then constructed by adding the T7 promoter sequence (5'TAATACGACTCACTATAG3') to the full-length shRNA sequence (Figure 2.2).

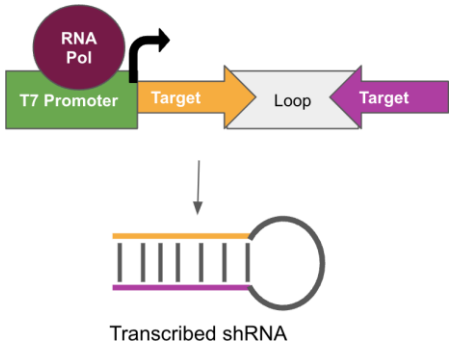

Figure 2.2: Schematic showing the in-vitro transcription of shRNA using a T7 RNA polymerase. Modified from Karabulut et al., 2019.

To prepare the shRNA *in vitro*, the forward and reverse primers were mixed in 1:1, annealed at 98°C for 5 minutes, and cooled to 24°C. The resulting duplex was used as a template for in vitro transcription by T7 polymerase using AmpliScribe™ T7-Flash Transcription Kit. The reaction was allowed to continue at 37°C overnight. DNase was then added for 30 minutes to remove the template, and the reaction mix was purified using Direct-zol™ RNA MiniPrep Plus.

2.2.3 Microinjection

Unfertilized de-jellied *Nematostella* eggs were microinjected using an Eppendorf FemtoJet 4x system. Glass capillary needles were pulled using Sutter Micropipette Puller P-87. The shRNA was diluted in nuclease-free water to a desired concentration, and 1µl of a tracer dye containing a 1:1 mixture of Dextran Red and FITC was added to prepare the injection mixture. Eggs were then fertilized with sperm water and cultured at 24°C until the desired stage.

2.2.4 Immunofluorescence

Planula larvae and polyps were briefly anesthetized with 7% $MgCl_2$ before fixation using 4% paraformaldehyde (PFA) in 12 ppt ASW for one hour at room temperature. Fixation was followed by five washes of five minutes each in phosphate-buffered saline + 0.1%

Tween-20 (PBSTw). For visualizing segment boundaries, fixed planula larvae were incubated in Phalloidin Alexa Fluor 488 (1:400) in PBS overnight at 4 ºC with overhead shaking. Hoechst 34580 was added (1:1000) as a nuclear marker.

Immunostaining with NvDlg was done using a custom antibody raised in rabbit. Planula larvae were fixed in 4% PFA in 12 ppt ASW and dehydrated to 100% MeOH by gradually washing them in 30% MeOH and 60% MeOH. At this point, samples can be stored in -20°C or used immediately. Samples were then rehydrated through 30% and 60% MeOH and washed into PBS + 0.2% Triton (PBSTx). Following three washes in PBSTx of five minutes each, samples were washed into Sodium Citrate buffer at pH 6.0 containing 0.05% Tween-20 and placed in a heat block at 97°C for 10 minutes. The samples were then brought to room temperature by placing tubes on a nutator for at least 20 minutes. After washing in PBSTx, blocking reagent (5% Goat Serum, 10% Roche Blocking Reagent, 10% DMSO in PBSTx) was added, and samples were placed at 4°C overnight. The primary antibody, NvDlg, was added in 1:300 and left for overnight incubation at 4°C. The next day, samples were washed in PBSTx, and an anti-rabbit 488 antibody was added for 2 hours at room temperature. Finally, the embryos were washed and incubated in Scale A2 (75% Glycerol + 2M Urea) at 4°C until imaged.

2.2.5 *In Situ* Hybridization (ISH):

The fluorescent *in situ* hybridization technique detects gene expression patterns in morphologically preserved embryos. It uses an *in vitro* synthesized RNA probe tagged with digoxigenin uridine-5’-triphosphate (Wolenski et al., 2013). Following hybridization, the target gene transcript is visualized using an anti-digoxigenin antibody (Figure 2.3).

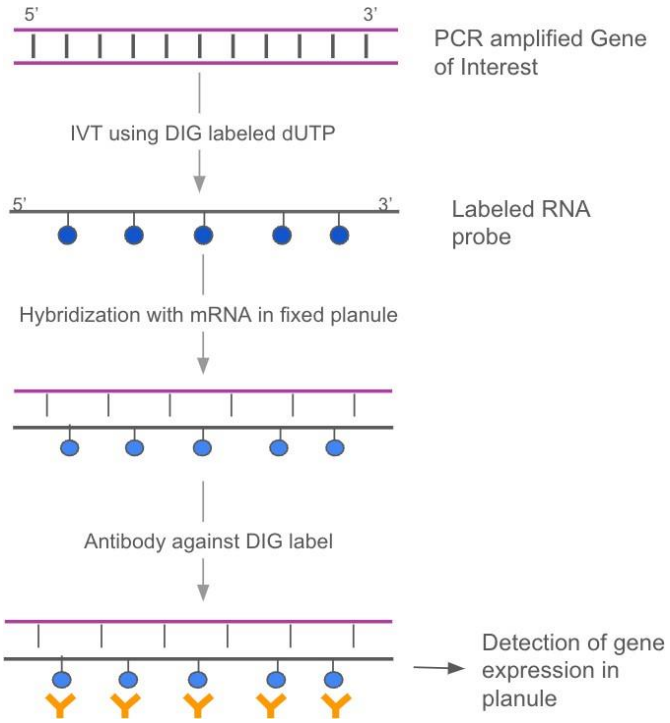

Figure 2.3: Steps of in-situ hybridization protocol for visualizing gene expression pattern

a. Preparing RNA probe:

NCBI Primer Blast was used to prepare the primers for synthesis of the DIG-labeled RNA probe, and the PCR product size was set to a minimum of 700 bp and a maximum of 1000 bp. Forward and reverse primers with low self-complementarity scores and similar GC content were selected so that the forward primer lies close to the start of the coding sequence region of the mRNA. The two primers were BLASTed against the *Nematostella* genome to check for specificity.

The synthesis of the DIG-labeled antisense RNA probe is done in-vitro using the T7 polymerase; therefore, the T7 promoter sequence was added to the reverse primer to create a third primer called the T7-reverse primer. All three primers were obtained from Integrated DNA Technologies (IDT).

As a first step in making the probes, cDNA was synthesized from wild-type planulae at 72 hours post-fertilization. The target gene was then amplified from the cDNA by the forward and reverse primers mixed in 1:1 using the Phusion PCR Kit. The reaction mixture was subjected to a PCR reaction of 35 cycles of denaturation at 95°C for 30 seconds, annealing at 56°C for 30 seconds, and extension at 72°C for 50 seconds. The PCR product was then purified and obtained using the Zymoclean Gel DNA recovery kit and the Zymo DNA clean & concentrator-5. Using the gel-purified product as a template, another identical PCR reaction was set up using the forward primer and the T7 reverse primer. This ensures that the T7 promoter region is added to the template to enable in-vitro transcription. Finally, the double-stranded PCR product with the T7 promoter region added to the gene of interest is used as a template to perform in-vitro transcription by the T7 polymerase. The DIG-RNA labeling mixture is added to the same reaction mixture. *In vitro* transcription is allowed to continue overnight at 37°C. DNase is added to digest the template the next day, and the RNA product is precipitated using 100% ice-cold ethanol. Ammonium acetate is added to allow maximum precipitation, and the tube is stored at -80°C overnight. The following day, the RNA probe is centrifuged at 4°C for 20 minutes, washed in 70% ethanol, and centrifuged at 4°C for 5 minutes. The step is repeated, and the precipitate is resuspended in 35µl of nuclease-free water. An equal amount of formamide is added, and the probe is stored at -20°C until used.

b. *In situ* hybridization (ISH)

Nematostella planulae at 72 hours post fertilization were fixed in 4% paraformaldehyde (PFA) in ASW for fluorescent in-situ hybridization (FISH) or in NAFA (Formic acid + 16% PFA + EGTA + 1M HEPES in 12 ppt ASW) for colorimetric in-situ hybridization (CISH) for 1 hour at room temperature and then washed with PBSTw (phosphate buffered saline + 0.1% Tween-20) five times for five minutes each. Samples were then dehydrated into 100% MeOH by gradually washing them in 30% MeOH and 60%MeOH in PBSTw. Fresh 100% MeOH was added to the samples and stored at -20 ºC until processed.

For *in situ* hybridization, samples were first photo-bleached by incubation in 3% H_2O_2 in 100% MeOH on a lightbox for 1hr, followed by rehydration through 60% and 30% MeOH. Embryos that were fixed with 4% PFA were then permeabilized by digestion with proteinase-K (20 µg/ml) for 10 minutes at room temperature without agitation. To stop the permeabilization, samples were incubated in 4% PFA in PBTw for 30 minutes at room temperature, followed by five washes in PBSTw for five minutes each. Permeabilization with Proteinase-K is not required for embryos fixed with NAFA. All samples are then incubated into a 1:1 mixture of PBTw and pre-hybridization buffer (pre-hybe) for 10 minutes, followed by incubation in 100% pre-hybridization buffer for 10 minutes at room temperature. Embryos were left overnight in the hybridization buffer (hybe) at 60ºC for blocking. Embryos were incubated in gene-specific RNA probes diluted in hybe buffer to a final concentration of 1.5ng/µl for 72 hours. Following hybridization, the samples were washed into 75%, 50%, and 25% of pre-hybe in 2X SSCTw (2X SSC + 0.1% Tween-20) before incubation in 100% 2X SSCTw. Samples were then washed in 0.2% SSCTw three times, followed by a single wash for 10 minutes at 60°C in a 1:1 mixture of SSCTw and PBTw for fluorescent in-situ hybridization or in a 1:1 mixture of SSCTw and MABTw buffer for colorimetric in-situ hybridization. Embryos were finally brought to room temperature and washed with PBSTw twice and three times in the TNT buffer for FISH. Embryos were brought to room temperature and washed in the MABTw buffer for CISH.

Finally, embryos were incubated in the blocking buffer (5% sheep serum + 1% Roche blocking agent + 10% DMSO in TNT buffer or in MABTw buffer) overnight at 4ºC. The next day, samples were incubated in Anti-DIG POD antibody (1:1000) for FISH and Anti-DIG AP antibody for CISH (1:2000) in the blocking buffer and kept overnight at 4°C. After incubation with the antibody, samples were washed ten times in the TNT buffer for FISH or in MABTw for CISH before developing the signal.

For fluorescent in-situ hybridization, to develop the signal, samples were incubated in TSA Cyanine 3 (Cy3) for 30 minutes away from light and then washed four times in the

TNT buffer, followed by four washes in PBTw. Nuclei were counterstained with Hoechst 34580 by incubating embryos overnight at 4ºC. Finally, the embryos were rinsed in PBTw and incubated in Scale A2 for mounting and imaging.

For colorimetric *in situ* hybridization, to develop the signal, samples were first washed in AP buffer without $MgCl_2$ (100mM NaCl + 50mM $MgCl_2$ + 100mM Tris (pH 9.5) + 0.1% Tween-20 in Milli-Q water) and then washed in AP buffer containing $MgCl_2$. Note that the AP buffer is filtered by a 0.45 µm filter before use. The development solution is prepared by adding 3.3 µL/mL NBT and 3.3 µL/mL BCIP in the AP buffer. Embryos are then moved into the development solution and incubated at room temperature, protected from light. The signal is checked every 30 minutes and samples are left at 4°C overnight if needed. To stop the signal development reaction, samples were washed in the AP buffer and finally incubated in 100% Ethanol to clear any background signal. Embryos were incubated in Scale A2 and stored at 4°C until imaged.

2.2.6 Imaging and Image Quantification

All images were taken using the Andor Dragonfly 200 Spinning Disk confocal microscope with FusionHD software. Images were later processed in Fiji to create a projection of multiple z-stacks for the purpose of visualizing segments.

CHAPTER 3: RESULTS

3.1 *Nematostella* Paraxis protein shares similarities with mouse and chicken

Phylogenetic analysis has shown that cnidarians possess most of the bilaterian orthologs of the bHLH family. The developmental importance of the bHLH transcription factor, *paraxis*, in mouse and chicken and its expression in the *Nematostella* endoderm leads us to believe that it plays an important role in establishing the *Nematostella* body plan. To understand the extent of conservation between bilaterian *paraxis* and its ortholog in *Nematostella*, an amino acid sequence alignment was done. Alignments at the level of proteins have been generally considered more useful (Abascal et al., 2010) as amino acids change more slowly through the course of evolution than their corresponding nucleic acids and are, therefore, easier to align. Moreover, the degeneracy of the genetic code and a smaller alphabet (4 nucleotides versus 20 amino acids) makes DNA sequences more prone to saturation than protein sequences. Lastly, the frequent substitution of amino acids with others of similar physical and chemical properties occurring throughout evolution is easily accounted for in protein sequence alignments.

The amino acid sequence of *Nematostella* Paraxis obtained from GenBank was aligned to that of Tcf15 (Transcription Factor 15 also known as Paraxis) from *Mus musculus* (mouse) and *Gallus gallus* (chicken) using ClustalW (Madeira et al., 2022) which uses an approach of aligning profile hidden Markov models (HMM), instead of the conventional dynamic programming alignment (Sievers & Higgins, 2018).

The *Nematostella* protein Paraxis shows 42% residue conservation with its mouse homologue and 45% with that of chicken (Figure 3.1(D)). The percentage of residue conservation is defined as the number of identical (‘matches’) residues between two sequences. It does not account for the amino acids that are similar in their physico-chemical properties but not identical.

The highly conserved region between the three sequences (Figure 3.1(C)) represents the functional bHLH domain (located at position 70 in the amino acid sequence of the mouse and position 61 in that of the chicken (Figure 3.1(A–B)). This suggests that the molecular role of Paraxis is likely to be conserved between cnidarians and bilaterians.

(A)

(B)

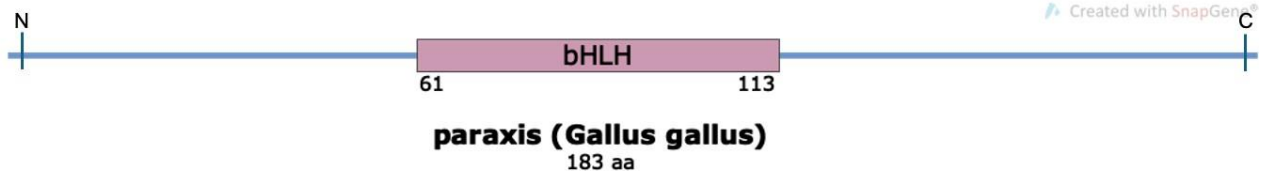

(C)

```
CLUSTAL O(1.2.4) multiple sequence alignment


NematostellaParaxis      --------------MEGTRRKREREQAPAVSEDDSDSSLKGSDSENA-------SRLKRK   39
MouseTcf15               MAFALLRPVGAHVLYPDVRLLSEDEEN-RSESDASDQSFGCCEGLEAARRGPGPGSGRRA   59
ChickenParaxis           MAFTMLRPMAARVLYPDIGMLSEDEEN-RSESDTSDQSYGCCEGAEARGKV---------   50
                                       .     * *:    ..* **.*   .:. :*

NematostellaParaxis      RRKPRLTGLSKQRQAANARERNRTHSVNAAFDALRLLIPTEPSDRKLSKIETLRLASSYI   99
MouseTcf15               SNGAGPVVVVRQRQAANARERDRTQSVNTAFTALRTLIPTEPVDRKLSKIETLRLASSYI   119
ChickenParaxis           PRKTGPMVMVKQRQAANARERDRTQSVNTAFTALRTLIPTEPVDRKLSKIETLRLASSYI   110
                          .      : :**********:**:***:** *** ****** **********************

NematostellaParaxis      AHLSTILISGTQCP-NVP-------SSMDHIRTISPSSARRVCTFCLSLLKAVTKDDKPL   151
MouseTcf15               AHLANVLLLGELTADDGQPCFRAAGGGKSAVPAADGRQPRSICTFCLSNQRKGGSRR-DL   178
ChickenParaxis           SHLANVLLLGEG-CEDGQPCFSSIYGAKGD---LDSKQPRSICTFCLSNQRKGGGRR-DL   165
                         :**:.:*: *     :         .. .     .  . * :******  :        *

NematostellaParaxis      SRNFM--------DRPRNRDSKS        166
MouseTcf15               GGSCLKVRGVAPLRGPRR-----        196
ChickenParaxis           GGNCLKVRGVTPLRVARR-----        183
                         . . :           *.
```

(D)

	1	2	3
1. Nematostella	100.00	42.14	44.97
2. Mouse	42.14	100.00	77.60
3. Chicken	44.97	77.60	100.00

Figure 3.1: (A-B) Map of the protein sequence in mouse and chick showing the position of the bHLH domain. Image created using SnapGene. (C) Amino acid sequence alignment obtained from ClustalW. The highly conserved sequence represents the bHLH region (indiacted in red). The asterisk (*) represents identical residues, a colon (:) represents residues with strongly similar properties (scoring > 0.5 on the Gonnet 250 matrix), and a period (.) indicates conservation between groups with weekly similar properties (scoring <= 0.5 on the Gonnet 250 matrix). (D) Percentage identity matrix. GenBank ID of protein sequences used - *Nematostella*: SJX71937.1, Mouse: AAA86825.1 and Chicken: AAC60208.1

3.2 Paraxis is expressed in *Nematostella* segments

To understand the expression pattern of *paraxis* in the endomesoderm, *in situ* hybridization was done using two different DIG-labeled RNA probes specific to the gene of interest (see materials and methods). The two probes are labeled ParaxisProbe(a) and ParaxisProbe(b) and amplify 614 bp and 721 bp of the *paraxis* gene, respectively (Figure 3.2). Both probes were BLASTed against the *Nematostella* genome to ensure gene specificity.

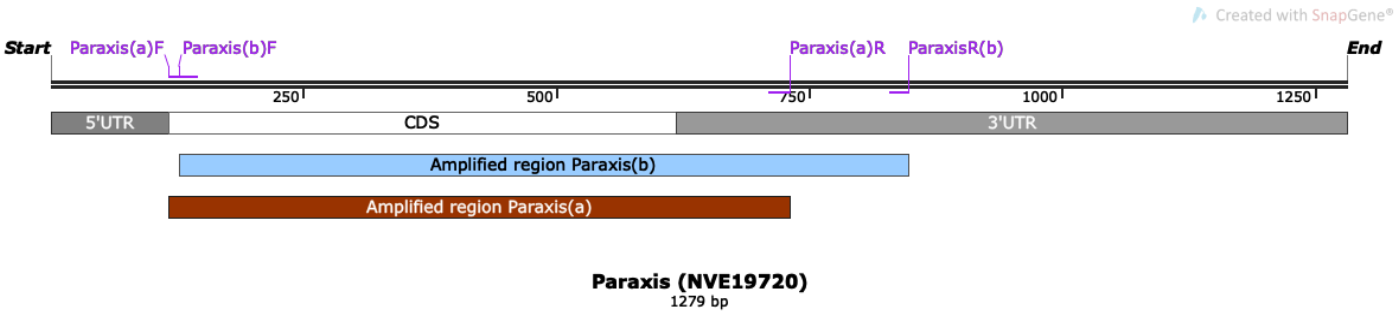

Figure 3.2: Map representing the region of the *paraxis* gene amplified by the two probes, Paraxis(a) and Paraxis(b). Created using SnapGene.

In fluorescent *in situ* hybridization (FISH), *paraxis* seemed to be ubiquitously expressed in all eight segments; however, it was absent from the segment boundaries, creating eight distinct domains of expression (Figure 3.3(A)). This is consistent with the expression pattern predicted by EndoAtlas (Figure 3.4(A)), an in-silico gene expression atlas that leverages single transcriptomics data to predict the expression pattern of genes computationally. However, the expression pattern was observed only with ParaxisProbe(a), whereas FISH using ParaxisProbe(b) showed non-specific hybridization and no true signal.

To determine if the signal observed with FISH using ParaxisProbe(a) was indeed the expression pattern of *paraxis* and not a result of some non-specific hybridization, a colorimetric *in situ* hybridization (CISH) was done using the same two probes (Figure

3.3(B)). Surprisingly, an expression pattern was observed with ParaxisProbe(b) but not ParaxisProbe(a). Without a nuclear marker, individual segments cannot be visualized in a colorimetric *in situ*. However, *paraxis* was expressed in all the segments of the endomesoderm.

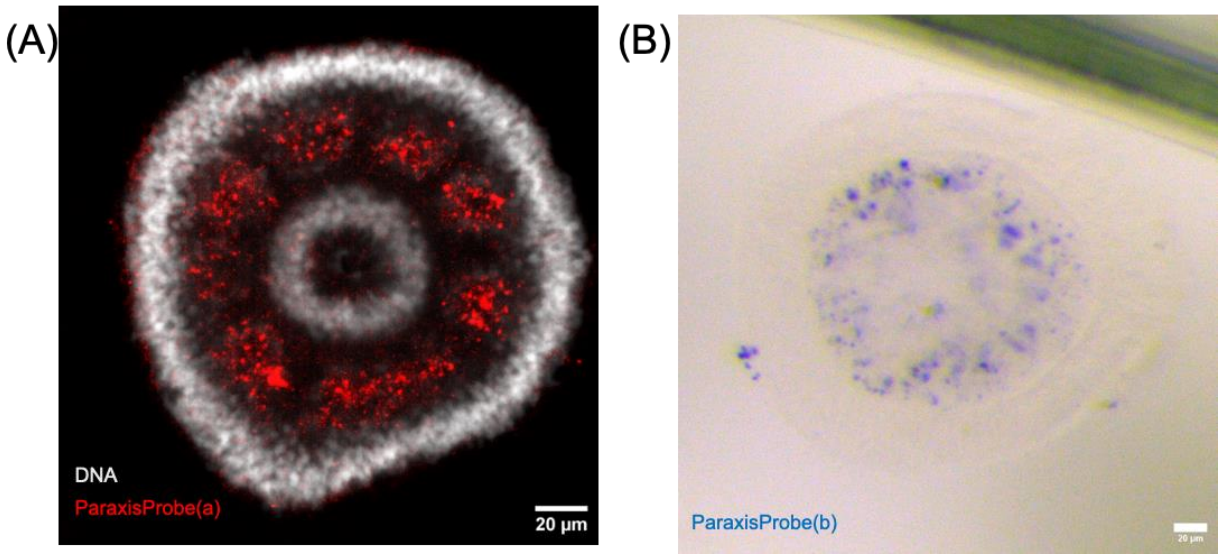

Figure 3.3: (A) Fluorescent in-situ hybridization showing the expression pattern obtained with ParaxisProbe(a) and (B) Colorimetric in-situ hybridization showing the expression pattern obtained with ParaxisProbe(b). Expression patterns were obtained in N = 3 for both FISH and CISH experiments.

While the *paraxis* expression pattern detected with the fluorescent and colorimetric in-situ experiments agrees with the spatially predicted expression pattern (Figure 3.4(A)), it is not consistent with the observations reported by Steinmetz et al., 2017, where *paraxis* appears to be unequally distributed across the segments with higher expression in some segments compared to others (Figure 3.4(B)). Further optimization of both probes would be required, and experiments will have to be repeated to produce replicates and improve the signal/noise ratio.

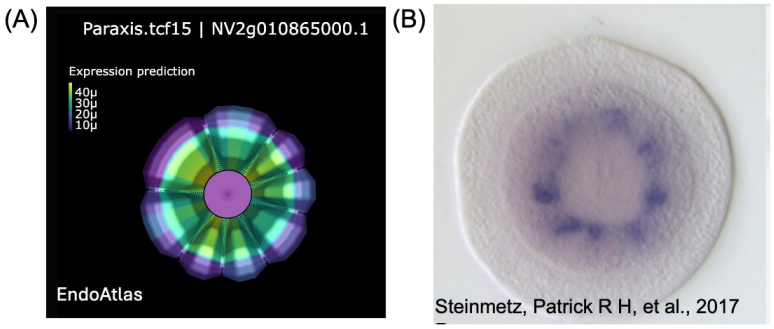

Figure 3.4: (A) Spatial predictions of *paraxis* expression pattern by EndoAtlas (He et al., 2023). (B) Whole-mount in situ hybridization by (Steinmetz, Patrick R H, et al., 2017) shows the expression of *paraxis* in the endoderm of the mid-planula stage larvae.

Although the precise spatial and temporal expression pattern of *paraxis* remains to be determined, it is clear that the gene is expressed within the endomesodermal segments at the planula stage and it might, therefore, play a role in regulating cell behavior during segmentation.

3.3 Segmental defects are observed in *paraxis* knockdown embryos

Since *paraxis* in mice is known to affect cell adhesion, cytoskeletal organization, and apical/basal polarity of epithelial somites, we suspected that it would play a role in the cellular organization of *Nematostella* segments. To test whether *paraxis* knockdown leads to segmentation defects, *Nematostella* planulae were stained with phalloidin at 72 hours post fertilization. Phalloidin binds to filamentous actin, which is enriched at the cell cortex and is, therefore, useful for visualizing cell boundaries and the apical surface of cells, making it ideal for visualizing segment boundaries (Cooper, 2000).

A wild-type *Nematostella* embryo, when imaged in the oral view, will show eight segments surrounding the central pharynx. In addition to staining the segment boundaries, phalloidin also marks the central cavity within each segment (Figure 3.5).

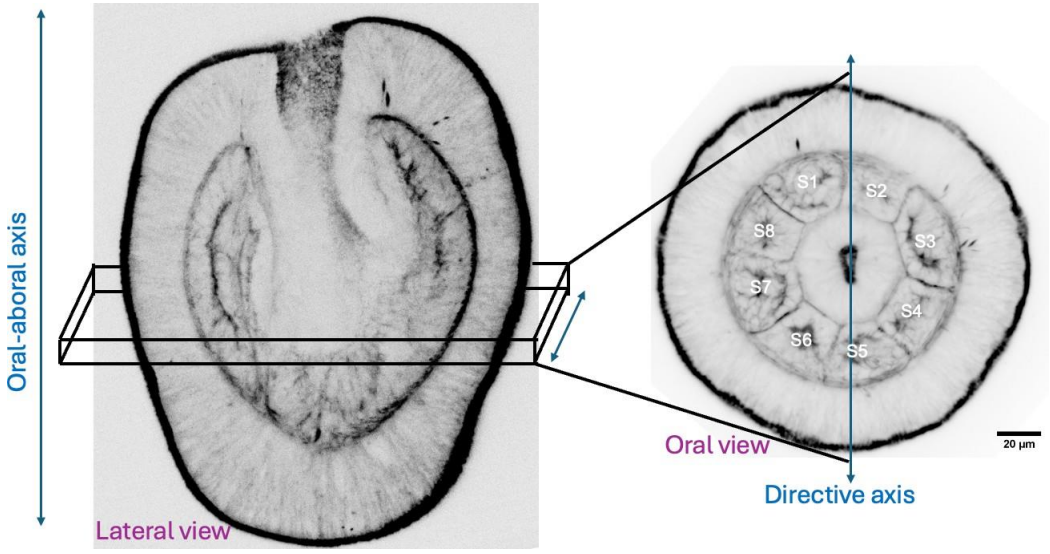

Figure 3.5: Phalloidin immunostaining of the lateral view and oral view of a wild-type Nematostella embryo at 72 hours post fertilization or 3 days post fertilization.

To create shRNA against *paraxis*, two 19 nucleotide regions of the *paraxis* mRNA were selected as targets. An shRNA for each of the two regions was created, resulting in two different shRNA - shParaxis1 and shParaxis2 (Figure 3.6). Each shRNA sequence was

BLASTed against the *Nematostella* genome to ensure gene specificity and eliminate off-target effects.

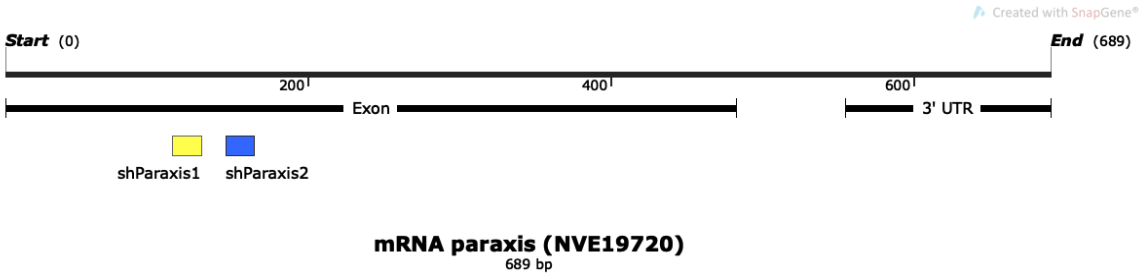

Figure 3.6: Sequence map for *paraxis* mRNA showing the two target regions used for creating the shRNA. Created using SnapGene.

Embryos injected with shRNA against *paraxis* showed segmental defects, including the fusion of segments resulting from a loss of segment boundaries and the formation of incomplete segment boundaries. A disruption in the shape of the pharynx and the boundaries between the pharynx and the segments can also be observed in most cases.

As a negative control to the experiments, to ensure that the phenotype observed does not arise from the method of injection, shRNA against eGFP was used; since it does not result in a gene knockdown, the wild-type phenotype of eight segments is expected. As a positive control, shRNA against *Anthox1a* was used, which resulted in the known phenotype of six segments arising from a fusion of segments - S4, S5, and S6 (He et al., 2018). Planulae showing defects in more than two segment boundaries have been classified as severe segmental defects, whereas planulae where exactly two segment boundaries are affected (as seen in *shAnthox1a* injected embryos) have been classified as having six segments. This classification was chosen to account for the phenotype observed in the positive control (six segments in *shAnthox1a*).

Figure 3.7 shows the segmental defects observed when one of the two target shRNA against *paraxis* (*shParaxis1*) was injected at an average final concentration of 500 ng/µl. A Fisher's exact test (Kim, 2017) was used to compare the frequency of total defects

observed in the injected sample with that of the uninjected (wild type) since the sample sizes are relatively small and vary for each group. For analysis, embryos containing severe segmental defects and six segments were combined into a single category labeled defects. A significant difference in defects was noted between embryos injected with *shParaxis1* at 500ng/µl and uninjected embryos (Figure 3.7(F))

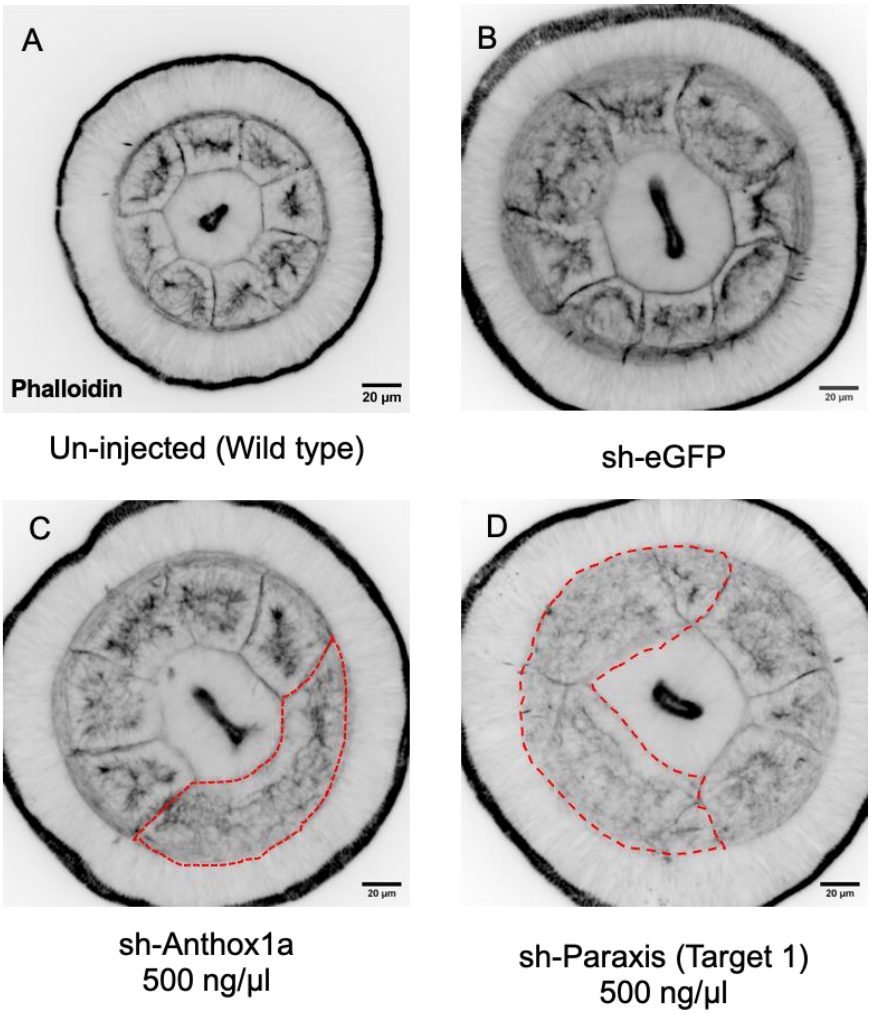

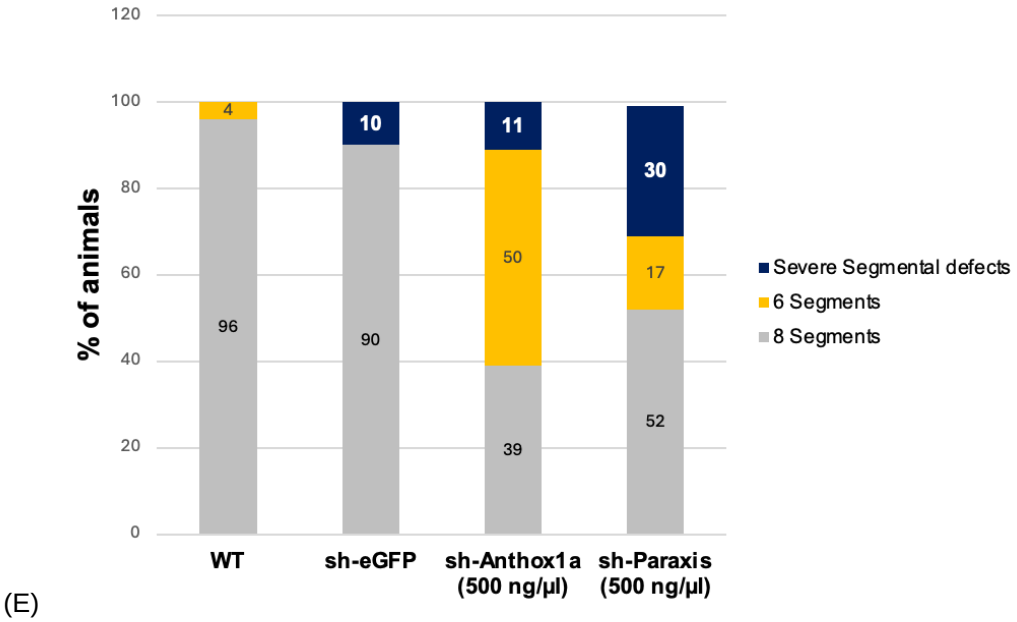

(E)

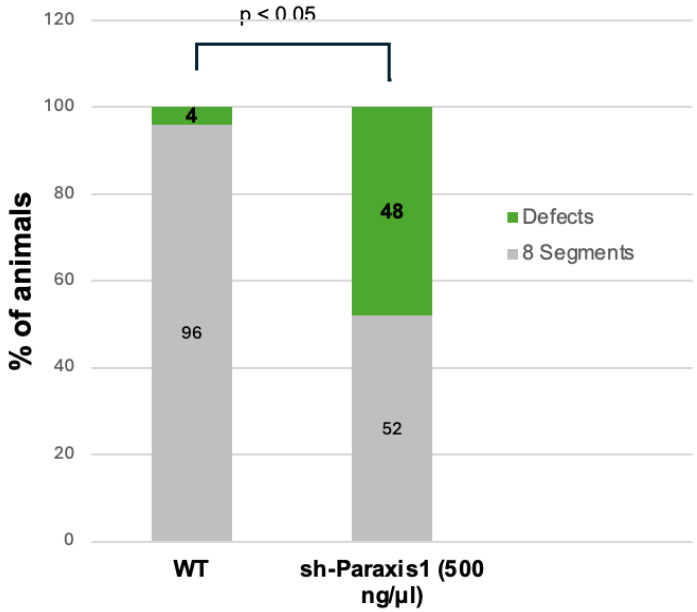

(F)

Figure 3.7: (A-C) Un-injected wild-type embryo showing eight segments along with a negative injection control sh-eGFP and positive injection control sh-Anthox1a showing eight and six segments, respectively. (D) Segmental defects (highlighted in red) were observed in embryos injected with shRNA against *paraxis* injected at 500 ng/µl. (E) The frequency of segmental defects and embryos with six segments observed in each category. (F) Defects observed in sh-paraxis embryos are significant compared to wild-type embryos, p-value = 0.006

To understand whether the percentage of defects observed depends on the final concentration of shRNA used in the injection mixture or the specific shRNA targeting another sequence, the experiments were repeated by injecting shRNA to an average final concentration of 900 ng/µl for each of the two target shRNA (*shParaxis1* and *shParaxis2*). Likewise, the concentration of the positive control, *shAnthox1a*, was also increased to 900 ng/µl. Interestingly, while the positive control, *shAnthox1a*, showed an increase in the frequency of expected phenotype (six segments) from the previous 50% to 74% upon using higher concentrations of shRNA, the percentage of severe segmental defects (Figure 3.8(C-D)) observed for *paraxis* remained at 36% and 32% for the two target shRNA (Figure 3.8(F)).

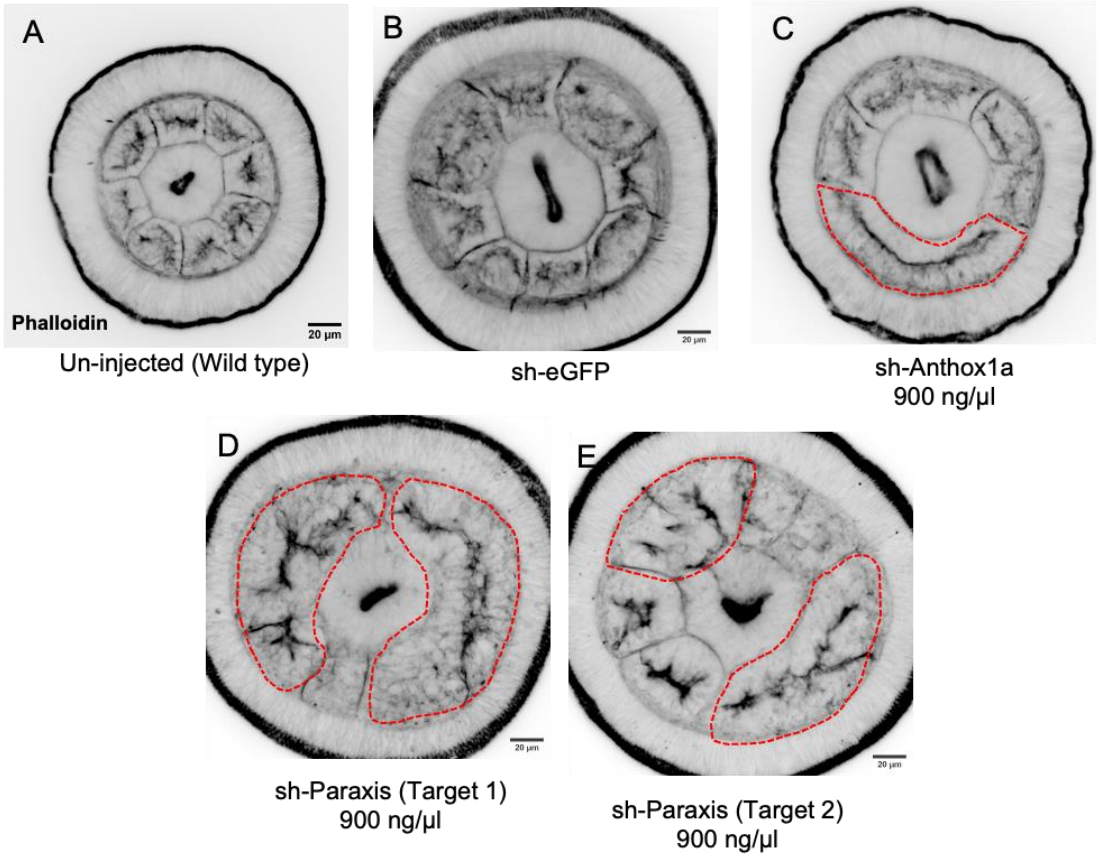

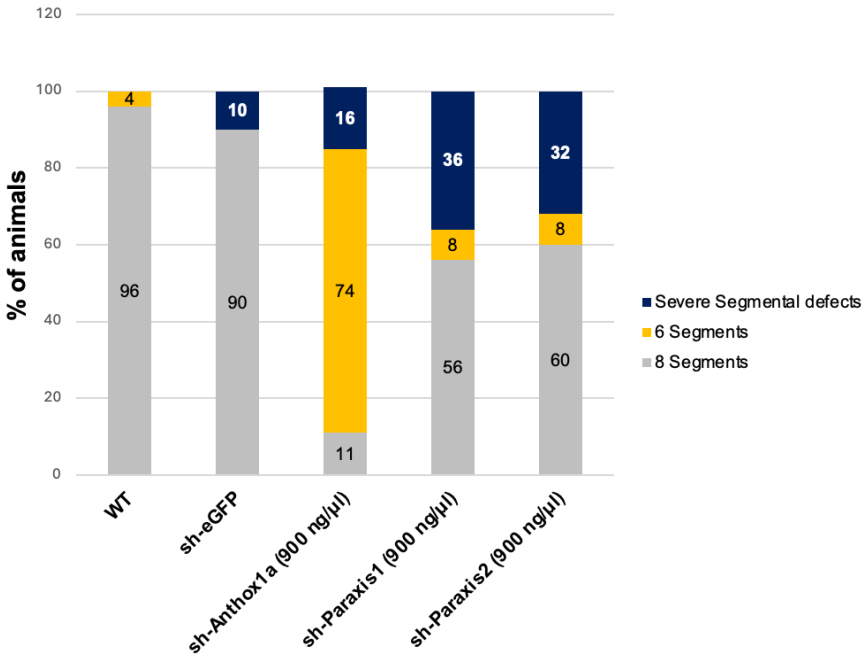

(F)

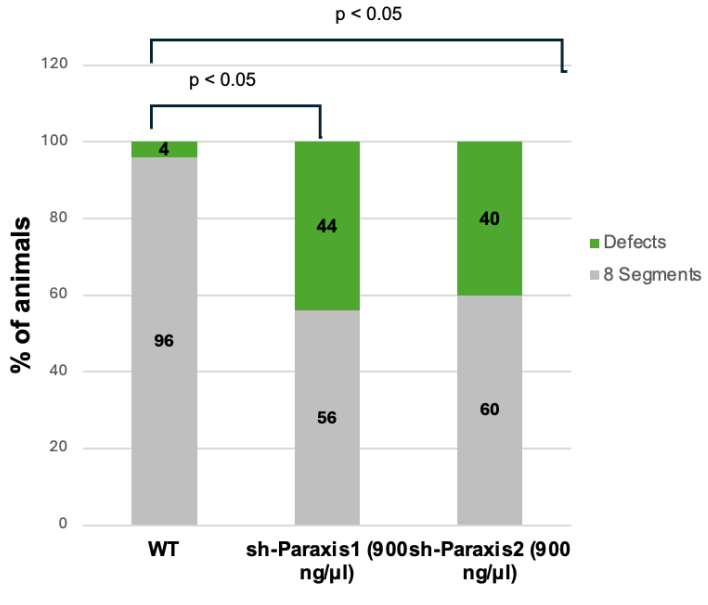

(G)

Figure 3.8: (A-C) Un-injected wild type embryo showing eight segments along with a negative injection control sh-eGFP and positive injection control sh-Anthox1a showing eight and six segments, respectively. (D-E) Segmental defects (highlighted in red) observed in embryos injected with shRNA against the first and second target region of *paraxis* mRNA injected at 900 ng/µl. (F) The frequency of segmental defects and embryos with six segments observed in each category. (G) Fisher's exact test analysis showed a significant difference between injected and uninjected embryos for both target shRNA. p-value = 0.001 and 0.004, respectively.

Finally, we performed knockdown analysis using an injection mixture diluted to a final concentration of 1200 ng/µl and containing both shRNAs against paraxis in equal concentration. Of the surviving embryos that were imaged, only 30% showed severe segmental defects (Figure 3.9).

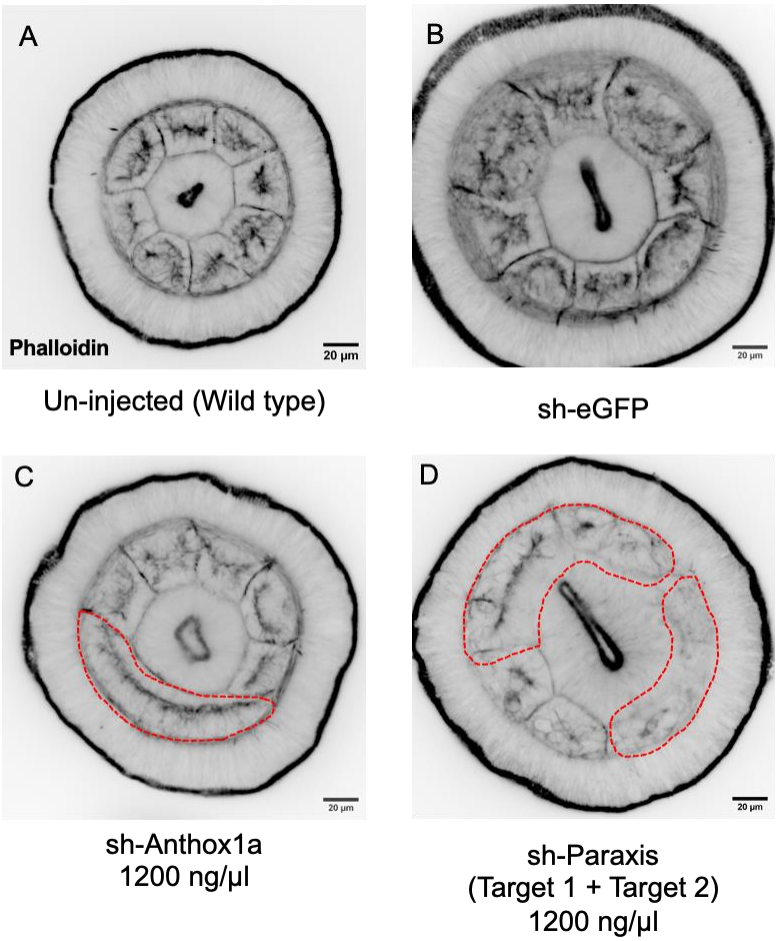

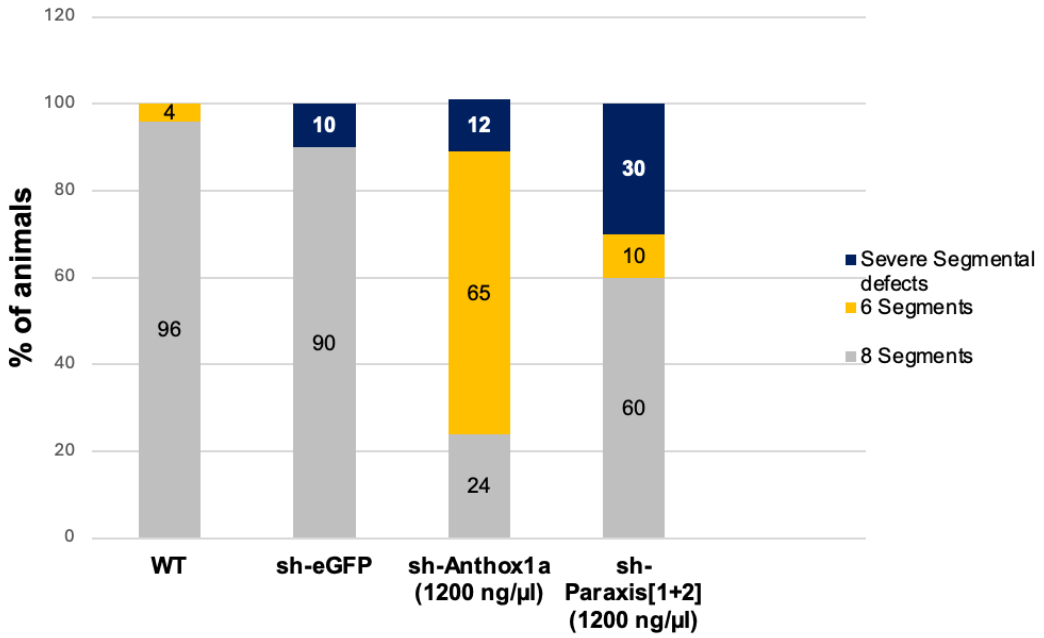

(E)

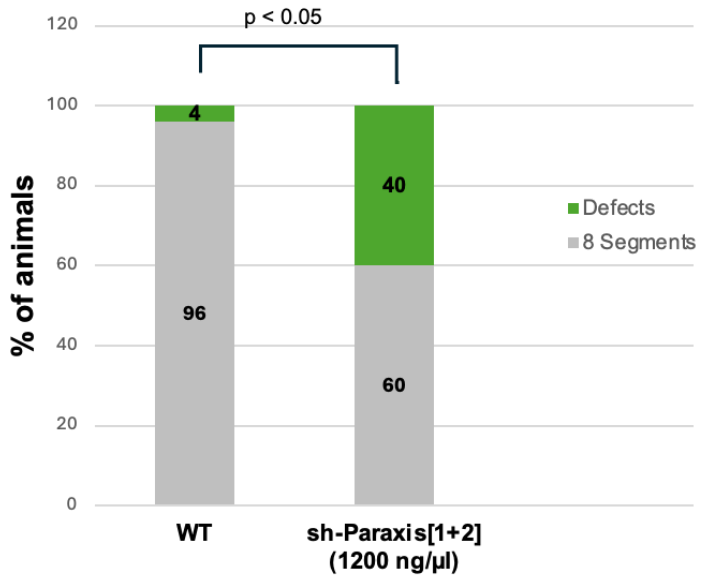

(F)

Figure 3.9: (A-C) Un-injected wild-type embryo showing eight segments along with a negative injection control sh-eGFP and positive injection control sh-Anthox1a showing eight and six segments respectively. (D) Segmental defects (highlighted in red) observed in embryos injected with a 1:1 mixture of two shRNA targeting two regions of the *paraxis* mRNA at 1200 ng/µl. (E) The frequency of segmental defects and embryos with six segments observed in each category. (F) The frequency of *paraxis-injected* embryos showing segmental defects is significant compared to uninjected, p-value = 0.006.

In summary, shRNA-mediated knockdown of *paraxis* led to total segmental defects (defined as any defects in formation of segment boundary) in an average of 42% of the embryos, irrespective of the final concentration of shRNA injected (Figure 3.10). However, the identity of the affected segments in the knockdown embryos could not be deduced. A summary of the phenotypes observed, and their frequencies are given in Table 3.1.

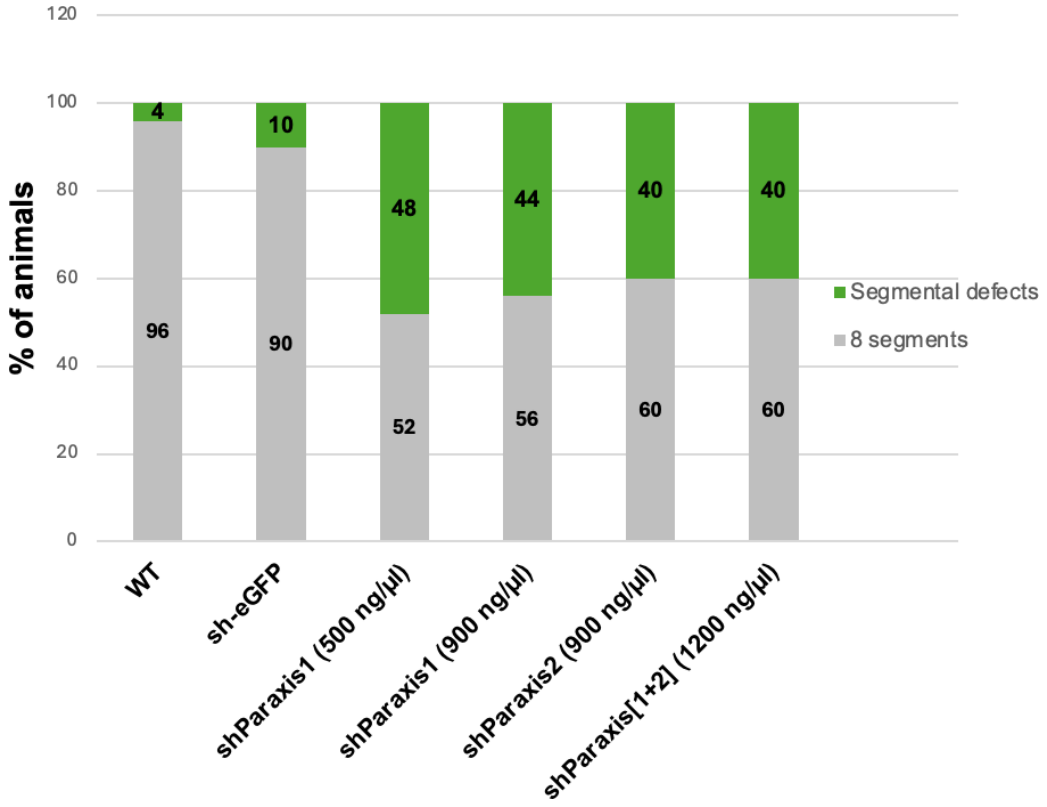

Figure 3.10: The frequency of total defects observed (embryos with two or more segment boundaries being affected) remains between 40% and 48%, irrespective of the shRNA injected.

Table 3.1: summarizing the phenotypes observed and their percentages:

shRNA	# embryos analyzed	Schematic of phenotype	Severe segmental defects	Six segments	Eight segments
WT	25	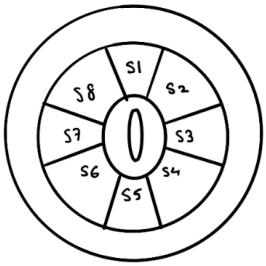	-	4%	96%
sh-eGFP	10		10%	-	90%
sh-Anthox1a (500 ng/µl)	18	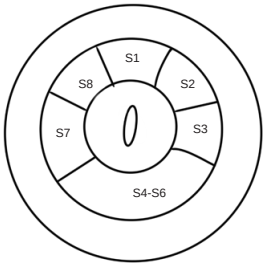	11%	50%	39%
sh-Paraxis1 (500 ng/µl)	23	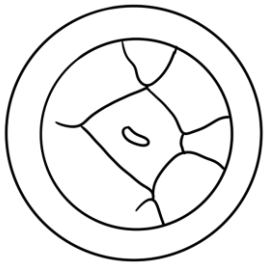	30%	17%	52%
sh-Anthox1a (900 ng/µl)	19		16%	74%	11%

sh-Paraxis1 (900 ng/µl)	25	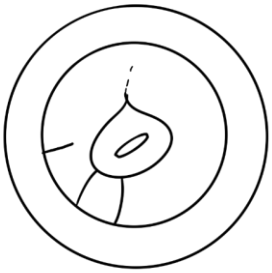	36%	8%	56%
sh-Paraxis2 (900 ng/µl)	24	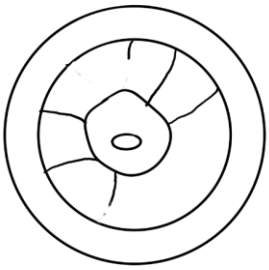	33%	13%	58%
sh-Anthox1a (1200 ng/µl)	17		12%	65%	24%
sh-Paraxis[1+2] (1200 ng/µl)	20		30%	10%	60%

3.4 Dlg is mislocalized in *paraxis* knockdown embryos

During development, embryonic cells must organize themselves into layers of polarized epithelia. The asymmetric distribution of cellular components, including proteins, cytoskeleton, and organelles, gives rise to distinct spatial domains within the cell, generating cell polarity (P. W. Miller et al., 2013; Rathbun et al., 2022). Cell-cell junctions such as adherens junctions ensure the mechanical binding between cells in the epithelial layer; in contrast, occluding junctions (tight junction and septate junctions) control paracellular transport across the epithelia (Ganot et al., 2015). Disruptions in cell-cell adhesion complexes and cell polarity lead to developmental defects.

Apico-basal polarity within epithelial cells is established by three highly conserved polarity complexes, Scribble, Par, and Crumbs, through a network of mutual antagonism. Members of these complexes have been identified in several non-bilaterian clades, and important functional domains are conserved between bilaterian and cnidarian organisms (Rathbun et al., 2022). Discs large (Dlg) is a component of the Scribble polarity complex and belongs to the membrane-associated guanylate kinase (MAGUK) family of scaffolding proteins (Roberts et al., 2012). Structurally, it contains three PDZ domains and one guanylate kinase domain, which are highly conserved. In the *Drosophila* epithelium, members of the Scribble polarity complex, including Dlg, are localized to the basolateral domain of the cell. Disruption of Dlg results in the disruption of the intercellular junction and loss of apical/basal polarity within epithelial cells. Similarly, in *C. elegans*, the Dlg homolog is required for proper formation of adherens junctions (Roberts et al., 2012).

A custom antibody against *Nematostella* discus large (NvDlg) was used to observe the effect of *paraxis* knockdown on the apico-basal polarity of cells within the segments. In wild-type and sh-eGFP injected embryos, NvDlg is localized such that segment boundaries are visible. However, the central lumen within the segments is not observed, suggesting that NvDlg localizes to the basolateral domain as observed in *Drosophila* and other bilaterians. On the other hand, NvDlg was mislocalized in *paraxis* knockdown

embryos. Similar to the phenotype observed in phalloidin stained embryos, a loss of segment boundaries was observed, and cells appeared to lose shape and become disorganized (Figure 3.11). The defects were observed in 40% of the imaged embryos, consistent with the segmental defects observed with phalloidin stained *paraxis* knockdown embryos. Together, the results from phalloidin and NvDlg immunostaining experiments suggest that *paraxis* is required for the proper organization of cells within segments.

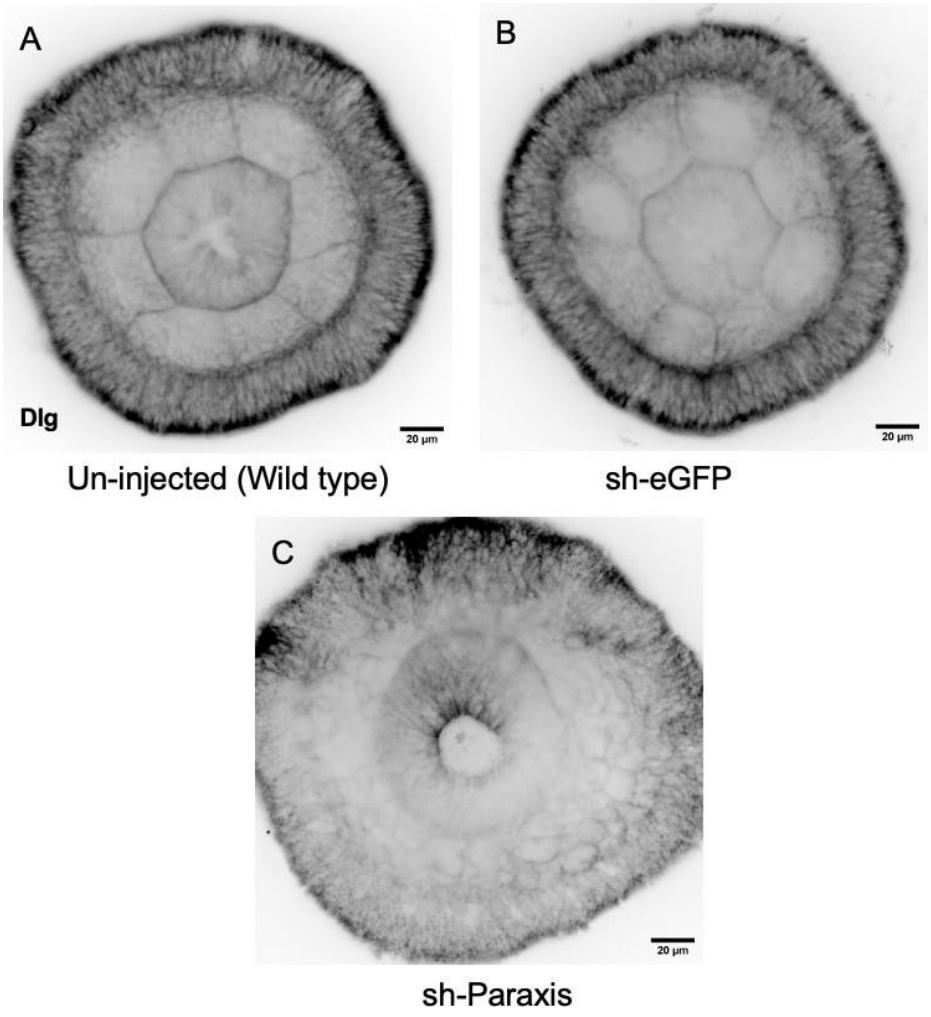

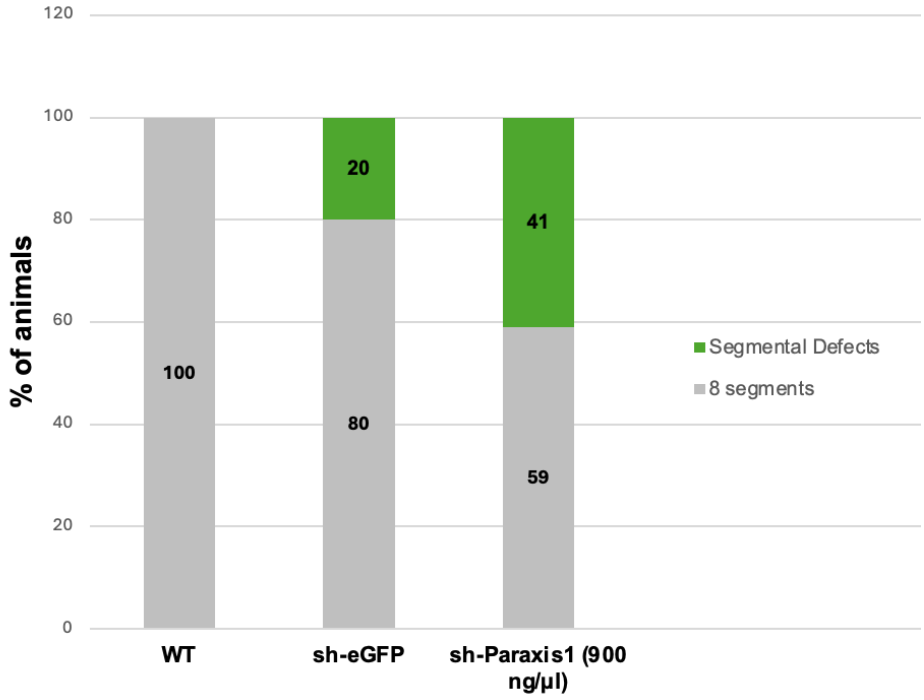

(D)

Figure 3.11: (A-B) Wild type embryo and sh-eGFP injected embryo (control) showing eight segment boundaries when stained with NvDlg. (C) No segment boundaries were seen in NvDlg stained paraxis injected embryos. (n = 3 for WT, 10 for sh-eGFP and 17 for sh-Paraxis. (D) Defects are observed in 41% of embryos that were imaged for shParaxis1 (900 ng/µl)

CHAPTER 4: DISCUSSION

4.1 Paraxis affects the cellular organization and morphology within *Nematostella* segments

The results presented in this thesis, although preliminary, suggest that *paraxis* is expressed in the endomesoderm segments of *Nematostella* and plays an important role in the cellular organization during segmentation. The shRNA-mediated knockdown experiments resulted in a loss of segment boundaries and disorganization of cellular morphology in an average of 42% of injected embryos. Whether the effect of *paraxis* on segment boundaries is direct or indirect remains to be studied. The frequency of defects observed was independent of the volume of shRNA injected. There are two possibilities for the low frequency of phenotype observed - either the efficiency of the shRNA in producing a knockdown is low irrespective of the concentration of shRNA used, or the penetrance of the phenotype is low. A quantitative polymerase chain reaction (q-PCR) validation will be required to test the efficiency of the knockdown produced by the shRNA.

Additionally, a CRISPR mutant containing a *paraxis* knockout will further the characterization and confirmation of the phenotype and enable the identification of the affected segments. Another possibility includes exploring the role of paralogs of the *Paraxis/Twist/Hand* related bHLH transcription factors in *Nematostella*, which might perform similar functions. Cole et al., 2023 have reported three bHLH factors, *nem7*, *nem24*, and *nem64*, which form a sea-anemone-specific paralog group clustered together with *paraxis* and *twist*. These paralogs have been implicated in the specification of muscle cell types. However, their function in segmentation remains unknown.

The interaction of *paraxis* with other genes, including upstream signals and downstream targets, remains to be studied. As a transcriptional activator, *paraxis* is likely to target

essential genes involved in regulating cell behavior. Future experiments, such as those resulting in RNA sequencing data from *paraxis* knockdown/CRISPR knockout animals and observing the effect of loss of *paraxis* on the expression of genes known to be involved in regulating cellular organization and morphology, will shed light on its downstream targets. This approach could be complimented with ChiP-seq approaches to elucidate global DNA binding sites for *paraxis*.

Studies in mice have predicted that *paraxis* functions downstream of the canonical Wnt signaling pathway and is likely to be activated by Wnt6 from the surface ectoderm (Rowton et al., 2013). However, the Wnt signaling pathway in *Nematostella* is known to pattern the oral-aboral axis (DuBuc et al., 2018; Linker et al., 2005). Its role in patterning the segments along the directive axis is largely unknown. In addition, forkhead/winged helix transcription factors, *FoxC1* along with *FoxC2,* are known to act upstream of *paraxis* in somite formation (Kume et al., 2001). Orthologs of *FoxC1* have been identified in the *Nematostella* endoderm, however, its interaction with other transcription factors remains to be studied. In addition to regulating somite epithelilization, downstream targets of *paraxis* in vertebrates function in specifying muscle identity (Wilson-Rawls et al., 1999). Likewise, sea-anemone-specific paralogs of *paraxis* drive muscle-cell type diversification (Cole et al., 2023). This suggests that the role of *paraxis* and the gene regulatory pathways it participates in might be evolutionarily conserved. However, experimental validation would be required to confirm this hypothesis.

4.2 Are *Nematostella* segments and vertebrate somites homologous?

Despite the morphological simplicity of *Nematostella*, its genome is surprisingly similar to that of vertebrates (D. J. Miller & Ball, 2008). It contains important developmental bilaterian gene families such as Wnt and Homeobox genes. The developing endoderm in *Nematostella* is enriched in genes whose bilaterian orthologs are involved in mesoderm specification and differentiation, as well as genes found in vertebrate somites (Steinmetz et al., 2017). This includes genes involved in somite epithelialization, such as *paraxis*; specificity of somite polarity, such as *Uncx*; genes involved in somite differentiation, such as *Meox;* and other genes involved in mesoderm patterning and myogenesis of bilaterians, including *FoxC1, Csrp2, and Mox* (He et al., 2023). Moreover, the role of the homeobox genes in defining segment identity is conserved between bilaterians and cnidarians.

Morphologically, *Nematostella* segments are similar to vertebrate somites as they are each clusters of cells patterned along a body axis, possess a segmental polarity, and differentiate into adult structures such as musculature.

The morphological and molecular parallels between *Nematostella* segments and vertebrate somites suggest the possibility of a common origin. This is in accordance with the enterocoel theory, which states that cnidarian segments represent a rudimentary form of vertebrate somites. Not all bilaterian lineages undergo segmentation through somitogenesis. For example, in the arthropod *Drosophila*, segmentation occurs through gradients of transcription factors. However, segmentation in arthropods and annelids is largely ectodermal, whereas it is mesodermal in vertebrates and *Nematostella*.

An alternative hypothesis is that the similarities observed between *Nematostella* segments and vertebrate somites result from convergent evolution and the two lineages independently evolved similar traits. It is possible that even if the *Nematostella* endoderm expresses gene orthologs of vertebral somites, they perform different

functions and participate in different regulatory and developmental pathways. In such a situation, *Nematostella* segments and vertebrate somites are likely similar because of convergent evolution and not a common origin. Future experimental evidence will be required to distinguish between the two hypotheses.

REFERENCES:

1. Abascal, F., Zardoya, R., & Telford, M. J. (2010). TranslatorX: Multiple alignment of nucleotide sequences guided by amino acid translations. *Nucleic Acids Research*, *38*(Web Server issue), W7-13. https://doi.org/10.1093/nar/gkq291
2. Burgess, R., Rawls, A., Brown, D., Bradley, A., & Olson, E. N. (1996). Requirement of the paraxis gene for somite formation and musculoskeletal patterning. *Nature*, *384*(6609), 570–573. https://doi.org/10.1038/384570a0
3. Carraco, G., Martins-Jesus, A. P., & Andrade, R. P. (2022). The vertebrate Embryo Clock: Common players dancing to a different beat. *Frontiers in Cell and Developmental Biology*, *10*. https://www.frontiersin.org/articles/10.3389/fcell.2022.944016
4. Cole, A. G., Jahnel, S. M., Kaul, S., Steger, J., Hagauer, J., Denner, A., Murguia, P. F., Taudes, E., Zimmermann, B., Reischl, R., Steinmetz, P. R. H., & Technau, U. (2023). Muscle cell-type diversification is driven by bHLH transcription factor expansion and extensive effector gene duplications. *Nature Communications*, *14*(1), Article 1. https://doi.org/10.1038/s41467-023-37220-6
5. Cooke, J., & Zeeman, E. C. (1976). A clock and wavefront model for control of the number of repeated structures during animal morphogenesis. *Journal of Theoretical Biology*, *58*(2), 455–476. https://doi.org/10.1016/S0022-5193(76)80131-2
6. Cooper, G. M. (2000). Structure and Organization of Actin Filaments. In *The Cell: A Molecular Approach. 2nd edition*. Sinauer Associates. https://www.ncbi.nlm.nih.gov/books/NBK9908/

7. DuBuc, T. Q., Stephenson, T. B., Rock, A. Q., & Martindale, M. Q. (2018). Hox and Wnt pattern the primary body axis of an anthozoan cnidarian before gastrulation. *Nature Communications*, *9*(1), Article 1. https://doi.org/10.1038/s41467-018-04184-x
8. Finnerty, J. R., Pang, K., Burton, P., Paulson, D., & Martindale, M. Q. (2004). Origins of Bilateral Symmetry: *Hox* and *Dpp* Expression in a Sea Anemone. *Science*, *304*(5675), 1335–1337. https://doi.org/10.1126/science.1091946
9. Fritzenwanker, J. H., Genikhovich, G., Kraus, Y., & Technau, U. (2007). Early development and axis specification in the sea anemone Nematostella vectensis. *Developmental Biology*, *310*(2), 264–279. https://doi.org/10.1016/j.ydbio.2007.07.029
10. Ganot, P., Zoccola, D., Tambutté, E., Voolstra, C. R., Aranda, M., Allemand, D., & Tambutté, S. (2015). Structural Molecular Components of Septate Junctions in Cnidarians Point to the Origin of Epithelial Junctions in Eukaryotes. *Molecular Biology and Evolution*, *32*(1), 44–62. https://doi.org/10.1093/molbev/msu265
11. Genikhovich, G., Fried, P., Prünster, M. M., Schinko, J. B., Gilles, A. F., Fredman, D., Meier, K., Iber, D., & Technau, U. (2015). Axis Patterning by BMPs: Cnidarian Network Reveals Evolutionary Constraints. *Cell Reports*, *10*(10), 1646–1654. https://doi.org/10.1016/j.celrep.2015.02.035
12. Genikhovich, G., & Technau, U. (2009). Induction of spawning in the starlet sea anemone Nematostella vectensis, in vitro fertilization of gametes, and dejellying of zygotes. *Cold Spring Harbor Protocols*, *2009*(9), pdb.prot5281. https://doi.org/10.1101/pdb.prot5281

13. Gibb, S., Maroto, M., & Dale, J. K. (2010). The segmentation clock mechanism moves up a notch. *Trends in Cell Biology*, *20*(10–2), 593–600. https://doi.org/10.1016/j.tcb.2010.07.001
14. Gilbert, S. F. (2000). Paraxial Mesoderm: The Somites and Their Derivatives. In *Developmental Biology. 6th edition*. Sinauer Associates. https://www.ncbi.nlm.nih.gov/books/NBK10085/
15. Gyoja, F. (2017). Basic helix-loop-helix transcription factors in evolution: Roles in development of mesoderm and neural tissues. *Genesis (New York, N.Y.: 2000)*, *55*(9). https://doi.org/10.1002/dvg.23051
16. He, S., del Viso, F., Chen, C.-Y., Ikmi, A., Kroesen, A. E., & Gibson, M. C. (2018). An axial Hox code controls tissue segmentation and body patterning in Nematostella vectensis. *Science*, *361*(6409), 1377–1380. https://doi.org/10.1126/science.aar8384
17. He, S., Shao, W., Chen, S. (Cynthia), Wang, T., & Gibson, M. C. (2023). *Spatial transcriptomics reveals a conserved segment polarity program that governs muscle patterning in Nematostella vectensis* (p. 2023.01.09.523347). bioRxiv. https://doi.org/10.1101/2023.01.09.523347
18. Hill, E. M., Chen, C.-Y., Del Viso, F., Ellington, L. R., He, S., Karabulut, A., Paulson, A., & Gibson, M. C. (2022). Manipulation of Gene Activity in the Regenerative Model Sea Anemone, Nematostella vectensis. *Methods in Molecular Biology (Clifton, N.J.)*, *2450*, 437–465. https://doi.org/10.1007/978-1-0716-2172-1_23
19. Ikmi, A., McKinney, S. A., Delventhal, K. M., & Gibson, M. C. (2014). TALEN and

CRISPR/Cas9-mediated genome editing in the early-branching metazoan Nematostella vectensis. *Nature Communications*, *5*, 5486. https://doi.org/10.1038/ncomms6486

20. Karabulut, A., He, S., Chen, C.-Y., McKinney, S. A., & Gibson, M. C. (2019). Electroporation of short hairpin RNAs for rapid and efficient gene knockdown in the starlet sea anemone, Nematostella vectensis. *Developmental Biology*, *448*(1), 7–15. https://doi.org/10.1016/j.ydbio.2019.01.005
21. Kelava, I., Rentzsch, F., & Technau, U. (2015). Evolution of eumetazoan nervous systems: Insights from cnidarians. *Philosophical Transactions of the Royal Society B: Biological Sciences*, *370*(1684), 20150065. https://doi.org/10.1098/rstb.2015.0065
22. Kim, H.-Y. (2017). Statistical notes for clinical researchers: Chi-squared test and Fisher's exact test. *Restorative Dentistry & Endodontics*, *42*(2), 152–155. https://doi.org/10.5395/rde.2017.42.2.152
23. Kume, T., Jiang, H., Topczewska, J. M., & Hogan, B. L. M. (2001). The murine winged helix transcription factors, Foxc1 and Foxc2, are both required for cardiovascular development and somitogenesis. *Genes & Development*, *15*(18), 2470–2482. https://doi.org/10.1101/gad.907301
24. Layden, M. J., Rentzsch, F., & Röttinger, E. (2016). The rise of the starlet sea anemone Nematostella vectensis as a model system to investigate development and regeneration. *Wiley Interdisciplinary Reviews. Developmental Biology*, *5*(4), 408–428. https://doi.org/10.1002/wdev.222
25. Layden, M. J., Röttinger, E., Wolenski, F. S., Gilmore, T. D., & Martindale, M. Q.

(2013). Microinjection of mRNA or morpholinos for reverse genetic analysis in the starlet sea anemone, Nematostella vectensis. *Nature Protocols*, *8*(5), 924–934. https://doi.org/10.1038/nprot.2013.009

26. Linker, C., Lesbros, C., Gros, J., Burrus, L. W., Rawls, A., & Marcelle, C. (2005). β-Catenin-dependent Wnt signalling controls the epithelial organisation of somites through the activation of paraxis. *Development*, *132*(17), 3895–3905. https://doi.org/10.1242/dev.01961
27. Madeira, F., Pearce, M., Tivey, A. R. N., Basutkar, P., Lee, J., Edbali, O., Madhusoodanan, N., Kolesnikov, A., & Lopez, R. (2022). Search and sequence analysis tools services from EMBL-EBI in 2022. *Nucleic Acids Research*, *50*(W1), W276–W279. https://doi.org/10.1093/nar/gkac240
28. Miller, D. J., & Ball, E. E. (2008). Cryptic complexity captured: The Nematostella genome reveals its secrets. *Trends in Genetics: TIG*, *24*(1), 1–4. https://doi.org/10.1016/j.tig.2007.10.002
29. Miller, P. W., Clarke, D. N., Weis, W. I., Lowe, C. J., & Nelson, W. J. (2013). The Evolutionary Origin of Epithelial Cell-Cell Adhesion Mechanisms. *Current Topics in Membranes*, *72*, 267–311. https://doi.org/10.1016/B978-0-12-417027-8.00008-8
30. Moran, Y., Fredman, D., Praher, D., Li, X. Z., Wee, L. M., Rentzsch, F., Zamore, P. D., Technau, U., & Seitz, H. (2014). Cnidarian microRNAs frequently regulate targets by cleavage. *Genome Research*, *24*(4), 651–663. https://doi.org/10.1101/gr.162503.113
31. Nejad Kourki, A. (2022). The integrative approach to inferring homology:

Morphology and development combined. *Biology & Philosophy*, *37*(4), 26. https://doi.org/10.1007/s10539-022-09846-1

32. Onai, T., Aramaki, T., Inomata, H., Hirai, T., & Kuratani, S. (2015). On the origin of vertebrate somites. *Zoological Letters*, *1*(1), 33. https://doi.org/10.1186/s40851-015-0033-0
33. Piatkowska, A. M., Evans, S. E., & Stern, C. D. (2021). Cellular aspects of somite formation in vertebrates. *Cells & Development*, *168*, 203732. https://doi.org/10.1016/j.cdev.2021.203732
34. Putnam, N. H., Srivastava, M., Hellsten, U., Dirks, B., Chapman, J., Salamov, A., Terry, A., Shapiro, H., Lindquist, E., Kapitonov, V. V., Jurka, J., Genikhovich, G., Grigoriev, I. V., Lucas, S. M., Steele, R. E., Finnerty, J. R., Technau, U., Martindale, M. Q., & Rokhsar, D. S. (2007). Sea anemone genome reveals ancestral eumetazoan gene repertoire and genomic organization. *Science (New York, N.Y.)*, *317*(5834), 86–94. https://doi.org/10.1126/science.1139158
35. Rathbun, L. I., Everett, C. A., & Bergstralh, D. T. (2022). Emerging Cnidarian Models for the Study of Epithelial Polarity. *Frontiers in Cell and Developmental Biology*, *10*, 854373. https://doi.org/10.3389/fcell.2022.854373
36. Roberts, S., Delury, C., & Marsh, E. (2012). The PDZ protein discs-large (DLG): The “Jekyll and Hyde” of the epithelial polarity proteins. *The FEBS Journal*, *279*(19), 3549–3558. https://doi.org/10.1111/j.1742-4658.2012.08729.x
37. Röttinger, E. (2021). Nematostella vectensis, an Emerging Model for Deciphering the Molecular and Cellular Mechanisms Underlying Whole-Body Regeneration. *Cells*, *10*(10), Article 10. https://doi.org/10.3390/cells10102692

38. Rowton, M., Ramos, P., Anderson, D. M., Rhee, J. M., Cunliffe, H. E., & Rawls, A. (2013). Regulation of mesenchymal-to-epithelial transition by PARAXIS during somitogenesis. *Developmental Dynamics*, *242*(11), 1332–1344. https://doi.org/10.1002/dvdy.24033
39. Saina, M., Genikhovich, G., Renfer, E., & Technau, U. (2009). BMPs and Chordin regulate patterning of the directive axis in a sea anemone. *Proceedings of the National Academy of Sciences of the United States of America*, *106*(44), 18592–18597. https://doi.org/10.1073/pnas.0900151106
40. Sánchez, R. S., & Sánchez, S. S. (2015). Paraxis is required for somite morphogenesis and differentiation in Xenopus laevis. *Developmental Dynamics*, *244*(8), 973–987. https://doi.org/10.1002/dvdy.24294
41. Sievers, F., & Higgins, D. G. (2018). Clustal Omega for making accurate alignments of many protein sequences. *Protein Science: A Publication of the Protein Society*, *27*(1), 135–145. https://doi.org/10.1002/pro.3290
42. Simionato, E., Ledent, V., Richards, G., Thomas-Chollier, M., Kerner, P., Coornaert, D., Degnan, B. M., & Vervoort, M. (2007). Origin and diversification of the basic helix-loop-helix gene family in metazoans: Insights from comparative genomics. *BMC Evolutionary Biology*, *7*, 33. https://doi.org/10.1186/1471-2148-7-33
43. Šošić, D., Brand-Saberi, B., Schmidt, C., Christ, B., & Olson, E. N. (1997). Regulation ofparaxisExpression and Somite Formation by Ectoderm- and Neural Tube-Derived Signals. *Developmental Biology*, *185*(2), 229–243. https://doi.org/10.1006/dbio.1997.8561

44. Stefanik, D. J., Friedman, L. E., & Finnerty, J. R. (2013). Collecting, rearing, spawning and inducing regeneration of the starlet sea anemone, Nematostella vectensis. *Nature Protocols*, *8*(5), 916–923. https://doi.org/10.1038/nprot.2013.044
45. Steinmetz, P. R. H., Aman, A., Kraus, J. E. M., & Technau, U. (2017). Gut-like ectodermal tissue in a sea anemone challenges germ layer homology. *Nature Ecology & Evolution*, *1*(10), 1535–1542. https://doi.org/10.1038/s41559-017-0285-5
46. Takahashi, Y., & Sato, Y. (2008). Somitogenesis as a model to study the formation of morphological boundaries and cell epithelialization. *Development, Growth & Differentiation*, *50*(s1), S149–S155. https://doi.org/10.1111/j.1440-169X.2008.01018.x
47. Tautz, D. (2004). Segmentation. *Developmental Cell*, *7*(3), 301–312. https://doi.org/10.1016/j.devcel.2004.08.008
48. Technau, U., & Genikhovich, G. (2018). Evolution: Directives from Sea Anemone Hox Genes. *Current Biology*, *28*(22), R1303–R1305. https://doi.org/10.1016/j.cub.2018.09.040
49. Technau, U., & Steele, R. E. (2011). Evolutionary crossroads in developmental biology: Cnidaria. *Development (Cambridge, England)*, *138*(8), 1447–1458. https://doi.org/10.1242/dev.048959
50. Ward, L., Evans, S. E., & Stern, C. D. (2017). A resegmentation-shift model for vertebral patterning. *Journal of Anatomy*, *230*(2), 290–296. https://doi.org/10.1111/joa.12540

51. Wikramanayake, A. H., Hong, M., Lee, P. N., Pang, K., Byrum, C. A., Bince, J. M., Xu, R., & Martindale, M. Q. (2003). An ancient role for nuclear β-catenin in the evolution of axial polarity and germ layer segregation. *Nature*, *426*(6965), Article 6965. https://doi.org/10.1038/nature02113
52. Wilson-Rawls, J., Hurt, C. R., Parsons, S. M., & Rawls, A. (1999). Differential regulation of epaxial and hypaxial muscle development by Paraxis. *Development*, *126*(23), 5217–5229. https://doi.org/10.1242/dev.126.23.5217
53. Wilson-Rawls, J., Rhee, J. M., & Rawls, A. (2004). Paraxis is a basic helix-loop-helix protein that positively regulates transcription through binding to specific E-box elements. *The Journal of Biological Chemistry*, *279*(36), 37685–37692. https://doi.org/10.1074/jbc.M401319200
54. Wolenski, F. S., Layden, M. J., Martindale, M. Q., Gilmore, T. D., & Finnerty, J. R. (2013). Characterizing the spatiotemporal expression of RNAs and proteins in the starlet sea anemone, Nematostella vectensis. *Nature Protocols*, *8*(5), Article 5. https://doi.org/10.1038/nprot.2013.014
55. Zhang, X., & Shu, D. (2021). Current understanding on the Cambrian Explosion: Questions and answers. *PalZ*, *95*(4), 641–660. https://doi.org/10.1007/s12542-021-00568-5